6-2017

AN ISOGENIC STEM CELL MODEL OF ALZHEIMER'S DISEASE: DIRECT EXPRESSION OF AMYLOID-BETA

Teresa Marie Ubina
California State University - San Bernardino, ubina.teresa@gmail.com

AN ISOGENIC STEM CELL MODEL OF ALZHEIMER'S DISEASE: DIRECT EXPRESSION OF AMYLOID-BETA

A Thesis

Presented to the

Faculty of

California State University,

San Bernardino

In Partial Fulfillment

of the Requirements for the Degree

Master of Science

in

Biology

by

Teresa Marie Ubina

June 2017

AN ISOGENIC STEM CELL MODEL OF ALZHEIMER'S DISEASE: DIRECT EXPRESSION OF AMYLOID-BETA

A Thesis

Presented to the

Faculty of

California State University,

San Bernardino

---

by

Teresa Marie Ubina

June 2017

Approved by:

Nicole Bournias-Vardiabasis, Committee Chair

Paul Salvaterra, Committee Member

Jeffrey Thompson, Committee Member

ABSTRACT

Alzheimer's disease (AD), identified over 100 years ago and intensively studied since the 1970s, has no effective treatments or mechanistic understanding of the underlying neurodegenerative process. Most investigators believe accumulation or aggregation of amyloid beta (Aβ) proteins plays a causative role. Aβ peptides (~39-43 residues) are generated by proteolysis of the transmembrane protein APP. One reason we know so little about AD is an incomplete understanding of the cellular mechanisms responsible for Aβ proteotoxicity. Human ES and iPSC models of AD are recent additions to many other models used to investigate these mechanisms. AD, however is a chronic progressive condition of old age and cultured neurons may not live long enough to model what goes wrong in neurons from AD patients. In my research, I used hESCs which directly express Aβ peptides thus avoiding the time it takes to process APP. One *App* allele in H9 hESCs was previously edited using TALEN. A homologous recombination cassette coding directly for a secretory form of either $A\beta_{1-42}$ or $A\beta_{1-40}$ and containing a stop codon, was inserted into the first exon of *App* upstream of the normal translational start site. I used multiple independently isolated clones of edited cells with 3 genotypes: *App*/*App* (unedited), *App*/$A\beta_{1-40}$ and *App*/$A\beta_{1-42}$. Expression of Aβ from edited alleles was confirmed by qRT-PCR using primers specific for the edit. I first sought to establish if editing changed any aspects of neuronal differentiation in culture. All 3 genotypes have similar embryoid body (EB) development, and similar numbers

and sizes of neuronal clusters (NC) up to 34 days after EB dissociation and neural differentiation. Immunostaining of neuronal markers, NeuN and DCX (doublecortin), likewise revealed no difference among edited and unedited cells, suggesting that the edits do not affect the ability of my stem cells to differentiate into neurons. I next measured accumulation of aggregated Aβ using an aggregate specific antibody, 7A1a. Data at 34-days post EB dissociation indicates NCs in the $A\beta_{1-42}$ edited cells accumulate significantly more aggregates relative to either unedited or $A\beta_{1-40}$ edited lines, a result consistent with the increased ability for $A\beta_{1-42}$ to form aggregates. Aβ aggregates also appear to be concentrated around fragmented nuclei within neuronal clusters suggesting that intracellular accumulation may play a key role in proteotoxicity. Additionally, I observed a significant decrease in the number of synapsin1 puncta, a marker of synapses, another feature of AD. I documented a nearly 3-fold greater neuronal cell death in both the $A\beta_{1-40}$ and $A\beta_{1-42}$ neurons at 70 days after differentiation. RNA sequencing data also shows independently isolated clones group together and show differential expression of genes related to memory and neuronal cell death. The early presence of Aβ aggregation and subsequent cell death is in line with the chronic and progressive nature of AD and this is the first known model to exhibit a neurodegenerative phenotype. These isogenic cell lines thus appear to be useful to screen for therapeutics that may prevent or slow $A\beta_{1-42}$ dependent neurodegeneration and a tool to investigate Aβ-dependent mechanisms with relevance to AD.

ACKNOWLEDGEMENTS

I would like to thank my mentor, Dr. Nicole Bournias-Vardiabasis, who helped me discover my love for the rigors of research and has always offered me opportunities, support, and fantastic advice not just in academics but also in life. I would also like to thank Dr. Paul Salvaterra for always challenging me to do better and for helping me to become a better scientist. I would like to thank the California Institute for Regenerative Medicine's Bridges program which granted me a generous stipend as well as funds for me to work at the Beckman Research Institute at City of Hope. I am thankful for the members of the Salvaterra lab, Martha Magallanes and Dr. Saumya Srivastava, for all of their help during my research. I would also like to thank Dr. Beer and everyone at the CSUSB Office of Student Research who have supported me in my research and made it possible for me to attend several conferences as well as expand my knowledge. Finally, I am thankful to my family and my husband who have always believed in me, pushed me to be better, and continue to support me throughout all my pursuits in life.

TABLE OF CONTENTS

LIST OF TABLES

LIST OF FIGURES

CHAPTER ONE

ALZHEIMER'S IS A CHRONIC, PROGRESSIVE, AND COMPLEX DISEASE

Background

Alzheimer's Disease (AD) is the most common form of dementia and the 6th leading cause of death in the United States ("FastStats - Leading Causes of Death," 2016). Symptoms include memory loss, cognitive impairment, behavioral changes, depression, and progressive neurodegeneration. The number of affected individuals is expected to increase almost four-fold by 2050 (Hebert, Weuve, Scherr, & Evans, 2013). While AD is devastating for patients, it also places burdens on their families, caregivers, and society. The average time from diagnosis to death is eight years and not every family has the insurance or financial resources to support the costs of long-term care often required for AD patients. While a patient's family can usually act as caregivers in the early stages of the disease, professional care or hospitalization is required as the disease progresses. The cost of long term care for patients is expensive and families frequently rely on inadequately funded public support programs. The emotional burdens belong only to the patient and their family but the financial burden is often shared by both the family and society.

Despite intensive research since the 1970s no cure or effective treatment has been found for AD. Part of the difficulty in finding an effective treatment lies with how little we understand about the mechanism of amyloid beta (Aβ) toxicity

in AD. This mechanism has been difficult to establish in part because accumulation of Aβ precedes its downstream pathological effects in the brain which may take decades to develop. An additional problem is that most laboratory AD models do not show significant neurodegeneration as part of their phenotype even though this is the major cellular aspect of the disease (Bales, 2012).

Neuropathology

Alois Alzheimer, in his discussion of his patient Auguste D., recognized two hallmark neuropathological lesions: senile plaques and neurofibrillary tangles (NFTs). These remain the best established post-mortem diagnostic criteria for AD. Plaques are primarily extracellular aggregates composed of several protein and non-protein components, but their major constituent is a small neurotoxic peptide called $A\beta_{1-42}$. NFTs are intracellular aggregates of a hyperphosphorylated form of microtubule associated protein tau.

Plaque numbers, despite being a hallmark lesion of AD, don't correlate strongly with AD symptoms such as memory loss or early stages of dementia. They accumulate in the brain of AD patients before tangles in both AD and AD models and are often a feature of non-affected brains in older individuals. Tangles, while correlating better with symptoms, are not unique to AD but are a characteristic lesion of many other neurodegenerative (ND) diseases referred to as tauopathies (Serrano-Pozo, Frosch, Masliah, & Hyman, 2011).

Proteolytic Production of Aβ

The $A\beta_{1-42}$ peptide found in plaques is generated by proteolysis of a large transmembrane protein, amyloid precursor protein (APP) along with several other Aβ peptides of differing length (39-43 amino acids) as well as other APP fragments (Haass, Kaether, Thinakaran, & Sisodia, 2012). The first step in the amyloidogenic pathway is cleavage of the extracellular domain by an enzyme called β-secretase. In the second step, a large 4 component protease, γ-secretase, cleaves the APP in the intramembranous region (Figure 1). The most common peptide is $A\beta_{1-40}$ along with $A\beta_{1-42}$. Significantly, rare autosomal dominant genetic forms of AD contain mutations in either the *App* gene itself or in two other genes (*Psen1* or *Psen2*) which form the active proteolytic site of γ-secretase. In addition to this pathogenic amyloid processing pathway there is an additional proteolytic pathway (non-amyloidogenic) which does not appear to be involved in AD. This non-amyloidogenic pathway starts with an initial cleavage of APP at a site within the N-terminus of $A\beta_{1-42}$ thus preventing Aβ formation via γ-secretase.

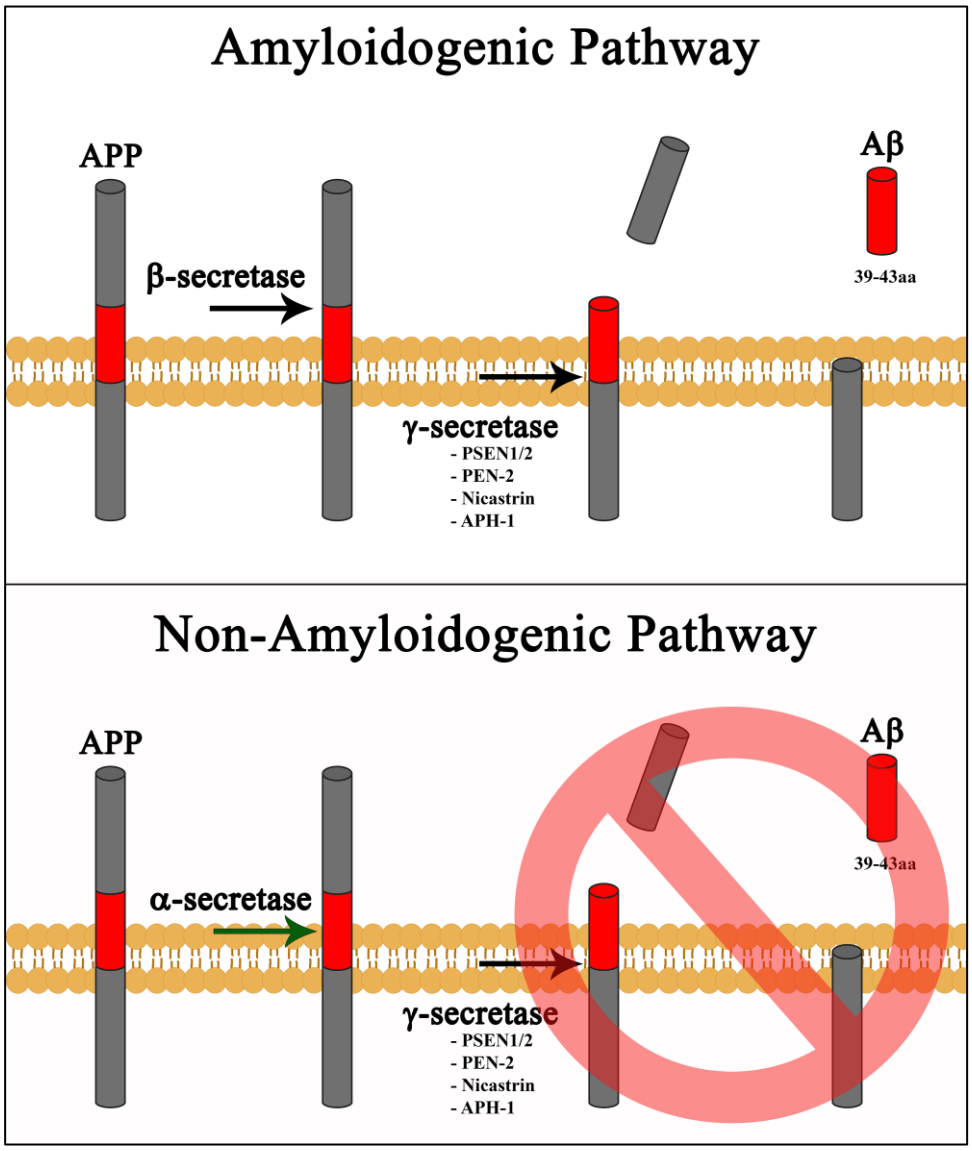

Figure 1. Aβ Formation via the Amyloidogenic Pathway.
In the amyloidogenic pathway β-secretase first cleaves APP and subsequently γ-secretase, resulting in 39-43 amino acid-long Aβ formation. The reason for the range in the length of Aβ peptides produced is that the active site in γ-secretase (PSEN1 or PSEN2) is not precise in its cleavage of APP, but the most common Aβ peptides formed are $A\beta_{1-40}$ and $A\beta_{1-42}$. In the non-amyloidogenic pathway (bottom), α-secretase first cleaves APP within the Aβ sequence which prevents subsequent cleavage by γ-secretase and Aβ formation.

Where is Aβ Produced?

Aβ is generated both extracellularly at the plasma membrane as well as intracellularly in the endoplasmic reticulum (ER), Golgi, lysosomes, and endosomes although the quantitative importance of production at these different sites is not known (Choy, Cheng, & Schekman, 2012; Hartmann et al., 1997; Sisodia, 1992).

Both $A\beta_{1-42}$ and $A\beta_{1-40}$ are known to form a variety of oligomeric and higher ordered aggregated structures. Many investigators believe that oligomeric $A\beta_{1-42}$ is the primary toxic form, consistent with its increased tendency to form aggregates relative to $A\beta_{1-40.}$ This may be a result of $A\beta_{1-42}$ being more hydrophobic by having an additional C-terminal Leucine and Alanine residues (Kang et al., 1987; Soto, Brahes, Alvarez, & Inestrosa, 1994). The mechanism of toxicity however is still not understood. Data is available for altered mitochondrial function, microtubule structure, ion channels, and various components of the intracellular membrane trafficking pathways such as autophagy, endosomal and lysosomal vesicles (C Ballatore, Lee, & J, 2007; Kanae Iijima-Ando et al., 2009; Lin, Bhatia, & Lal, 2001; Martinez-Vicente, 2015). Aβ production as well as aggregation is consistently observed in intracellular vesicles but it is still debated if this compartment plays a primary role in toxicity or if the extracellular Aβ plaques are more important. Notably, conditions favorable for in vitro Aβ oligomerization include a high concentration of Aβ peptide and an acidic environment, both of which are not likely present in extracellular compartments

but common in intracellular organelles such as lysosomes and late endosomes (Hu et al., 2009). Additionally, intracellular Aβ accumulation appears before extracellular accumulation and the ER is the main site of intracellular Aβ oligomerization (Meli et al., 2014; Oddo, Caccamo, Smith, Green, & LaFerla, 2006).

Tau Tangle Formation and Its Pathological Appearance in AD

Tau, also known as neuronal microtubule associated protein tau, normally plays a role in the outgrowth of neuronal processes by promoting microtubule stability and assembly (Z. Liu et al., 2015). Association of tau with microtubules is mostly dependent on its phosphorylation status. Unphosphorylated tau attaches readily to microtubules and promotes their stability. Phosphorylation of Tau causes separation from microtubules which allows cellular cargo to pass (Carlo Ballatore, Lee, & Trojanowski, 2007). Hyper-phosphorylation of tau at specific sites creates unstable microtubules and cytoplasmic tau begins to form paired helical filaments that aggregate into NFTs within the cell (Z. Liu et al., 2015; Virginia M.-Y. Lee, Brian J. Balin, Laszlo Otvos, 1991).

While both Aβ plaques and NFTs likely contribute to neuronal death, Aβ accumulation as well as plaque formation precedes and may even induce NFT formation (Götz, Schild, Hoerndli, & Pennanen, 2004). Immunotherapy studies in mice targeting Aβ and reducing its accumulation also result in a reduction in the levels of intracellular phosphorylated tau (Frank M LaFerla, 2010). Following cessation of immunotherapy Aβ pathology reappears before NFTs.

Vesicular Accumulation in AD

Abnormal accumulation of vesicles is another well documented pathological hallmark of AD, as well as many AD models (Nixon, 2006). These vesicles often express markers of autophagy, endosomal and lysosomal (AEL) subcellular compartments and may thus be fusions of these ordinary types of vesicles. Aggregated Aβ is present within AEL vesicles both intracellularly as well as in extracellular space (Ihara, Morishima-Kawashima, & Nixon, 2012). Neurons normally experience a high rate of vesicular turnover and the increase in number as well as size of AEL vesicles in AD or models suggests that their turnover efficiency is diminished and they are thus dysfunctional (Ling, Magallanes, & Salvaterra, 2014). Fusion of endosomes or autophagosomes with lysosomes is considered the end stage leading to vesicular cargo digestion allowing the digested components to be reused for cellular biosynthetic functions. In AD and AD models the vesicular fusion pathways apparently still operate normally but the cargo is no longer being digested thus preventing vesicular turnover.

The Genetics of AD

AD can be divided into two general forms: sporadic (SAD) and familial (FAD). Like its name suggests, FAD exhibits an autosomal dominant inheritance pattern as a result of causative mutations in one of three genes present in two or more generations of relatives (Kovacs & Tanzi, 1998). There are no distinguishing characteristics of FAD and SAD other than the observation that FAD patients develop symptoms at a relatively younger age (also known as early

onset AD, EOAD). The three genes mutated in FAD are *APP*, *Presenilin 1* (*PSEN1*), and *Presenilin 2* (*PSEN2*) (Bertram, Lill, & Tanzi, 2010). FAD mutations in *APP* can be located within the $A\beta_{1\text{-}42}$ sequence but are usually located at or very near the cleavage sites of α-secretase or β-secretase (Weggen & Beher, 2012). Either PSEN1 or PSEN2 forms the active site of a four subunit protease complex, γ-secretase, necessary for amyloidogenic processing of APP into Aβ (Zheng & Koo, 2011). All known forms of FAD result in more efficient production of $A\beta_{1\text{-}42}$ over $A\beta_{1\text{-}40}$ providing the strongest evidence in favor for the amyloid hypothesis of AD: $A\beta_{1\text{-}42}$ is causative (Selkoe & Hardy, 2016). Additional evidence comes primarily from transgenic mouse models of AD where agents known to slow or prevent APP proteolysis into $A\beta_{1\text{-}42}$ (or even remove $A\beta_{1\text{-}42}$ aggregates) generally decrease the severity of AD-like phenotypes in these models (Vardy, Catto, & Hooper, 2005). Unfortunately, it has not yet been possible to translate these findings into patient treatments as all clinical trials based on these mouse models have failed. Recent versions of the amyloid hypothesis postulate that the production and aggregation of $A\beta_{1\text{-}42}$ may cause subsequent plaque formation, tau tangle formation, and subsequently neurodegeneration but the mechanistic details involved are still poorly understood.

In addition to *APP*, *PSEN1*, and *PSEN2*, genome wide associated studies in individuals diagnosed with AD have identified several genes associated with a higher incidence of AD risk (Lambert et al., 2013). The earliest identified and

quantitatively most important among these is the presence of a risk allele of *apolipoprotein E* (*APOE*) (Kanekiyo, Xu, & Bu, 2014). *APOE* has three alleles (ε2, ε3, and ε4). Individuals carrying just one copy of ε4 have up to a four-fold increase in the likelihood of developing AD and copies correlates with an increased risk by almost fifteen-fold (Farrer et al., 1997). Interestingly, *APOE ε4* carries an increased risk in both FAD and SAD (Liu, Kanekiyo, Xu, & Bu, 2013)(C.-C. Liu et al., 2013). APOE normally functions in cholesterol metabolism. APOE4 promotes oligomerization of Aβ peptides and is also found in tangles (Castano et al., 1995). Other studies as well as our own genomic sequencing data shows the H9 cell line used in our model is heterozygous ε3/ ε4 (Funk et al., 2012).

Current Models

The most common models of AD are constructed in mice, invertebrates, or cell lines. The predominant models used for preclinical development of AD treatments are transgenic mice (Frank M. LaFerla & Green, 2012). Mouse models have been extremely successful in identifying the proteolytic processing mechanisms for production of Aβ as well as accumulation of plaques, but they have been less successful in modeling other types of AD pathology. Most extensively studied mouse models rely on overexpression of one or more mutant forms of a human AD causative transgene. Some models even use additional mutations in other genes not known to be affected in AD to achieve AD-related phenotypes. Notably, FAD patients have only a single mutation in one of the

three causative genes (*APP, PSEN1, PSEN1*) while SAD cases have no known cause. It is thus hard to interpret transgenic mouse results with respect to AD.

Perhaps the two biggest phenotypic deficiencies in nearly all mouse models is the absence of significant neurodegeneration and the lack of tangles (Alzforum, 2016). More recent mouse models were designed to replace the endogenous mouse *App* gene with a copy of a mutant human gene. This strategy has eliminated potential problems caused by overexpression, but these animals still require human APP processing using mouse proteins and neurodegeneration has not been reported (Saito et al., 2014).

Invertebrate models of AD often rely on direct expression of $A\beta_{1-42}$ transgenes (Gutierrez-Zepeda & Luo, 2004; K Iijima-Ando & Iijima, 2009). This strategy results in models exhibiting an impressive array of AD-like phenotypes including selective accumulation of $A\beta_{1-42}$, chronic age-dependent neurological deficiencies, and significant neurodegeneration (Cowan, Shepherd, & Mudher, 2010; Kanae Iijima-Ando & Iijima, 2010).

One drawback is that they share an absence of tangle formation just as in mouse models. Remarkably, a few mouse models have also been examined using direct expression of $A\beta$ and they share the robust neurodegeneration phenotypes with invertebrates but are not widely used or no longer available (Abramowski et al., 2012; LaFerla, Tinkle, Bieberich, Haudenschild, & Jay, 1995; Lewis et al., 2001). Though animal models have given us a great deal of knowledge about AD, the species differences between humans and animals are

increasingly being appreciated and could play a significant role in the limitations of current AD models.

An obvious way to overcome species differences is to create human embryonic stem (hES) or induced pluripotent stem (iPS) cell models of AD. Two general approaches have been used: converting iPSCs from AD patient derived cells into neurons or genomic editing to introduce AD mutations into hES or iPS cells. The first strategy has been used by several groups with promising results (Kondo et al., 2013; Yagi et al., 2011; Yang, Li, He, Cheng, & Le, 2016).

One drawback of iPSC studies is the absence of a proper control cell line. Age matched non-AD cells have been used but these are likely to have a host of genetic variants that may complicate simple direct interpretations of AD-like phenotypes. This can be avoided by using genetic editing technologies. However, it is still difficult to imagine how cell models can be experimentally analyzed long enough to view age-dependent changes. Most stem cell culture experiments last for a few months at the most and AD takes decades to develop in humans (McGowan, Eriksen, & Hutton, 2006). Some progress has be made in solving these aging problems, primarily by stressing the cells or incorporating expression of genes with accelerated aging phenotype (Studer, Vera, & Cornacchia, 2015). My model has taken a different approach. First, genetic variance is limited by using a standard well characterized human embryonic stem cell as a starting point. Second, my cells have been genomically edited to directly express a secretory form of Aβ thus avoiding the time it would take to

proteolytically process APP peptide. This strategy also allows phenotypic characterization of $A\beta_{1-42}$ and $A\beta_{1-40}$ separately, something impossible to do in APP models. $A\beta_{1-40}$ which is largely non-toxic in invertebrate direct expression models and less toxic in mouse direct expression models. The $A\beta_{1-42}$ edited cell lines I observed thus have the potential to serve as an editing control. While not specifically a model of AD per se, we hypothesize that this system of isogenic lines will represent a new tool that can be used to understand the consequences of $A\beta_{1-42}$ accumulation that result in AD-like neurodegeneration. The final feature of these cells is that the edits are incorporated into the *App* gene itself and is thus not an overexpression model but rather relies on expression control from the normal App regulatory elements.

Constructing a New Human ES Cell Based Model

All cell lines used in this study were derived from the well-defined and established WA09 hESC line (referred to herein as H9). Multiple independently isolated clones were established following transcription activator-like effector nuclease (TALEN) genomic editing. We targeted a sequence in the first exon upstream of the translation initiation site in *App* by designing TALEN pairs that introduce a double strand break (DSB). The DSB was repaired in the presence of a plasmid containing a cassette constructed of a left and right homology arm (flanking the targeted cutting site), a secretory signal sequence (from the *R.rattus* preproenkephin gene), either an $A\beta_{1-40}$ or $A\beta_{1-42}$ coding sequence followed by a

drug selection gene and a polyA tail using normal homology directed repair. This resulted in a secretory form of either $A\beta_{1-42}$ or $A\beta_{1-40}$ peptide under the control of the normal *App* promoter. The secretory signal directs expression routing through the normal secretory pathway as known for APP and the secretory signal is completely removed during normal secretory processing. Multiple independently isolated clones were obtained and examined for each edit ensuring that results are genotype specific and not likely a result of unknown modifications during editing. PCR analysis and direct sequencing of the editing junctions confirmed all edited cells. Expression of the edited genes can be specifically monitored by qRT-PCR using a forward primer in the rat secretory sequence that is not present in the human genome. Details of sequences and methods used to construct this model can be found in Appendix A.

CHAPTER TWO

NEURONAL DEVELOPMENT

App and Aβ Insert Expression

It is important to first establish the level of mRNA in edited samples for both the edit itself as well as the remaining unmodified *App* allele. While the exact function of APP is not known, a few reports have claimed a role in early development. I therefore measured both *Aβ* expression and *App* expression using qRT-PCR throughout development. There is a significant decrease in both $A\beta_{1\text{-}40}$ and $A\beta_{1\text{-}42}$ mRNA comparing stem cells to embryoid bodies (Figure 2). The pattern and extent of decrease appears similar for each edit. Following dissociation of EBs and differentiation into neurons there is a large increase in Aβ expression and the pattern is similar for each edit, however, $A\beta_{1\text{-}40}$ appears to express more peptide mRNA (Figure 2).

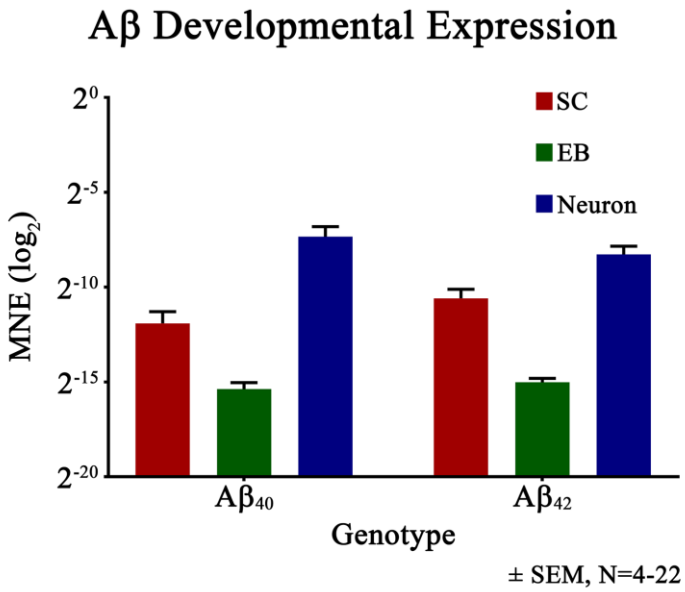

Figure 2. Expression of $A\beta_{1\text{-}40/42}$ Inserts at Different Developmental Stages.
Expression of Aβ inserts was measured by qRT-PCR using primers in the secretory signal sequence which cannot be found in the human genome. In both cell lines, expression decreases from stem cells to neurons by ~24-fold. In $A\beta_{1\text{-}40}$, expression from EB to neurons increased by ~308-fold. Expression in $A\beta_{1\text{-}42}$ from EB to neurons increased by ~107-fold. Overall, both genotypes increase expression of the Aβ insert from SC to neuron by ~14-fold.

App expression also showed a similar pattern comparing $A\beta_{1\text{-}40}$ and $A\beta_{1\text{-}42}$ NCs. As expected, expression of *App* in edited lines was approximately half the expression relative to unedited H9 cells (Figure 3). Somewhat unexpectedly, expression of the *Aβ* edited mRNA was ~37-fold less than *App* in edited genotypes relative to the unedited H9 cell line (Figure 3). This may potentially be

explained by functional disruption of an *App* enhancer sequence reported within the first intron of the gene as a result of cassette insertion in this region (Shakes et al., 2012). This reduced expression may in fact be beneficial since $A\beta_{1-42}$ peptide has acute proteotoxic properties and lower expression may allow development of more chronic toxicity as the peptide slowly accumulates as the neurons age, a situation similar to AD. In any case, the *Aβ* mRNA levels are indistinguishable from background in unedited cells.

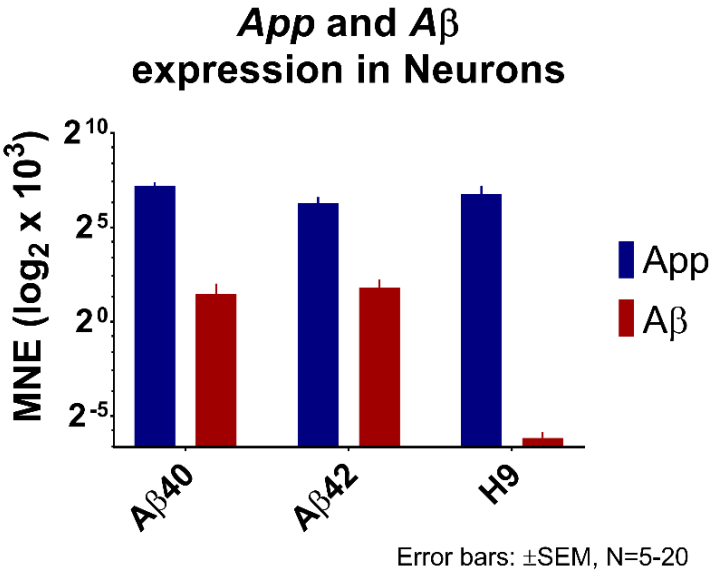

Figure 3. Expression of *App* and Aβ in Neurons of All Three Genotypes.
App expression in my $A\beta_{1-42}$ and $A\beta_{1-40}$ neurons is near half the expression of H9 neurons and not significantly different from each other. Expression of the $A\beta_{1-40}$ and $A\beta_{1-42}$ inserts are both 37-fold less than their respective *App* expressions.

Alzheimer's is Not a Developmental Disease

AD is not considered a developmental condition but rather a phenotype of old age. Before evaluation of direct Aβ-dependent phenotypes in my cell lines it is crucial to first determine if they can differentiate normally. After EB dissociation, neurons begin to migrate into organized neuronal clusters (NC). These clusters grow larger as a function of culture time and eventually develop extensive neuronal processes and form synaptic connections within a particular cluster and apparently with adjacent NCs. Upon visual inspection using Hoffman differential interference microscopy, the neurons and NCs of unedited or either edited genotype appear similar in morphology and increase in size as they age (Figure 4). I compared the average area of NCs among all three genotypes at 6-15 days, 16-25 days, and 26-35 days. Data were collected across independent differentiations to control for normal variability in culture morphologies. The average area of NCs appeared to increase. Statistical analysis of pooled data from multiple differentiations (ANOVA corrected for multiple comparisons using Dunnett's method), however, failed to reach significance. There can be several potential technical reasons for this statistical anomaly. For example, it may have been better to measure volumes of NCs rather than area. The most likely reason, however, is that within a particular neuronal differentiation the increase in NC size is obvious but when pooling data form different individual neuronal differentiations the variations are greater than the increase in NC area. Ideally, this possibility could be tested by increasing the number of individual neuronal

differentiations however this was not possible due to time and expense considerations. The source of variation in stem cell differentiation is a well-known problem in stem cell biology of unknown cause.

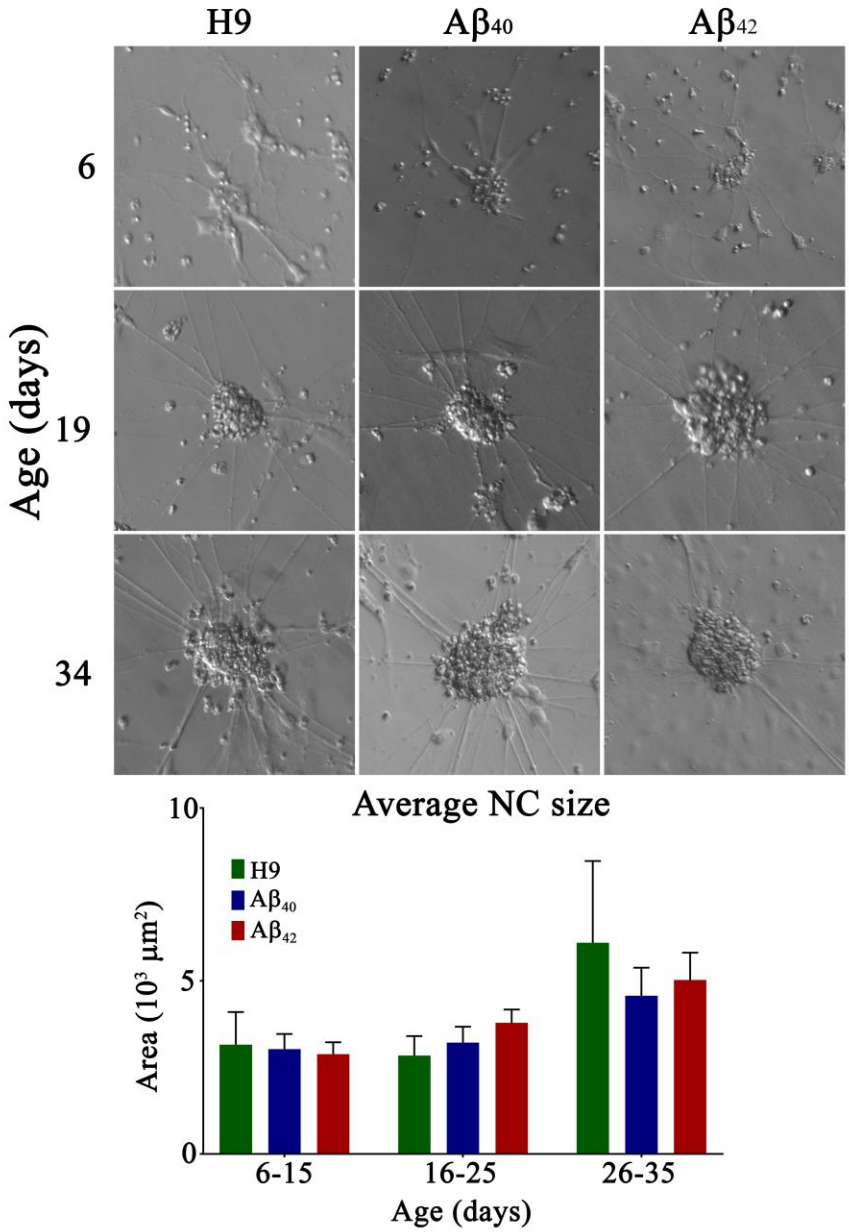

Figure 4. Neuronal Clusters Appear Similar and Grow Larger As They Age. The appearance of the NCs of all three genotypes is similar up to 34 days and grow slightly larger as they age (top). The sizes of neuronal clusters at different age ranges were measured by manually tracing around the boundaries and measuring the area of several clusters within each culture. When the average areas are compared at each age range using ANOVA (with Dunnett's multiple comparisons) there was no statistically significant difference.

To determine if the edits made to my cells affected the number of neurons that ultimately develop, I immunocytochemically stained and imaged 10 day old neurons AED (after embryoid body dissociation) for two neuron specific markers that are localized within two different cellular compartments. The first, NeuN, is a nuclear neuronal marker and the second, doublecortin (DCX), is a cytoplasmic neuronal marker. The neurons of all three genotypes at 10 days AED appear so similar in number and morphology that it is difficult to distinguish them (Figure 5). When the percentage of positive staining cells is compared among H9, $A\beta_{1-40}$, and $A\beta_{1-42}$ following image analysis, I find that there is no statistical difference for NeuN positive or DCX positive cells (Figure 5).

Taken together, the results in this section suggest that all 3 genotypes analyzed can develop and differentiate normally (i.e. similar to the H9 parental genotype) and thus phenotypic analyses at later stages may be confidently predicted to be a result of edited peptide expression rather than effects on earlier developmental processes.

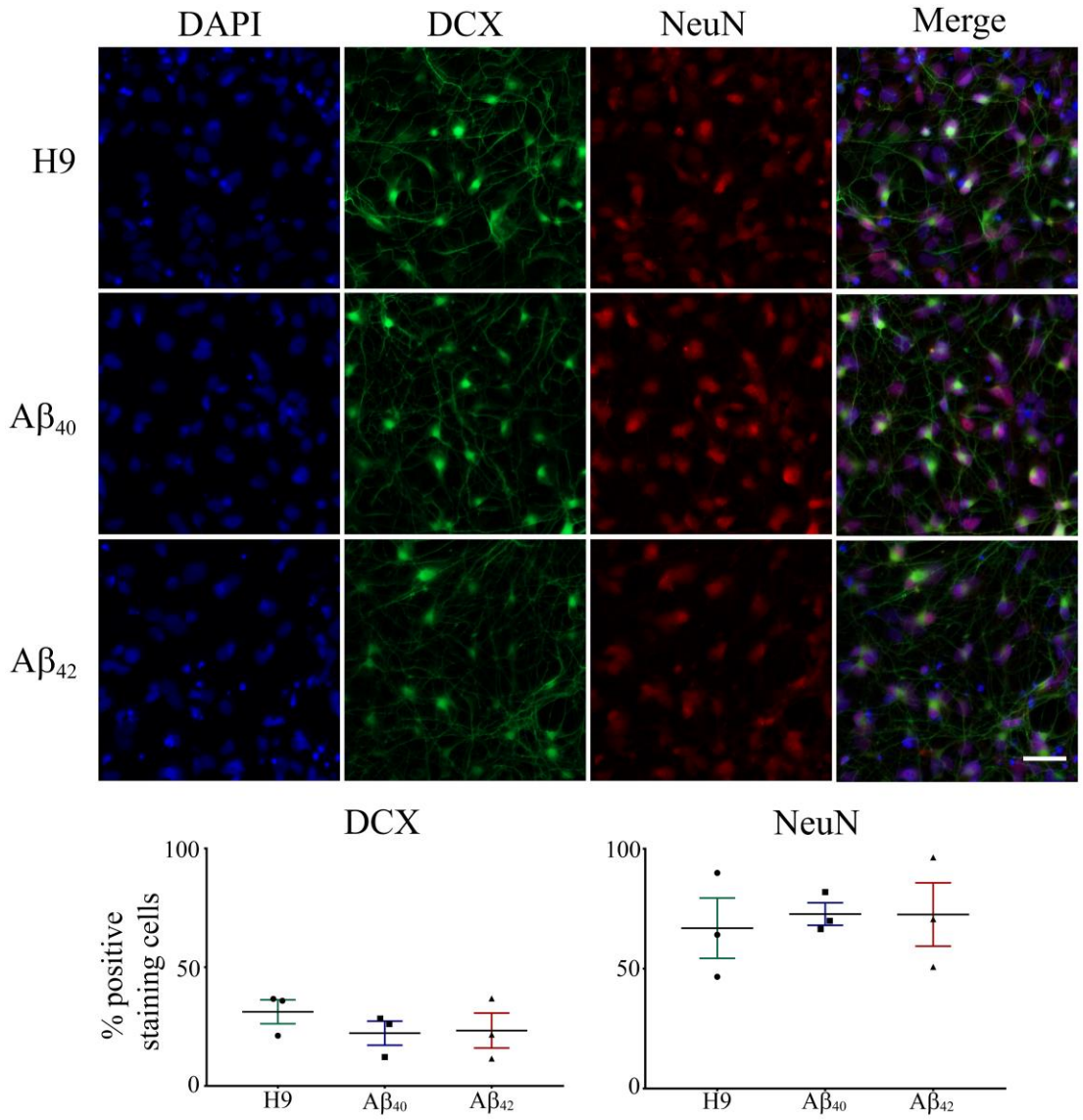

Figure 5. Edits Do Not Affect the Number of Neurons That Develop After Differentiation.
Neurons were immunocytochemically stained for two neuronal markers, doublecortin (DCX) and NeuN 10 days AED. The number of cells positive for each type of neuronal marker were counted in several fields and the percentages of positive cells were compared. There was no difference by visual comparison in morphology and number (top) as well as by statistical analysis (bottom, ANOVA with Dunnett's multiple comparisons test, N=15-38). Scale bar 30µm.

CHAPTER THREE

ALZHEIMER'S-LIKE PHENOTYPES

Aβ Aggregation

An early hallmark of AD is aggregation and accumulation of the $A\beta_{1-42}$ peptide and thus measuring the aggregation of Aβ is a logical first step in examining differentiated neurons in my cultures. Aβ aggregation was measured immunocytochemically by staining 32-34 day old (AED) cultures with an antibody specific for the aggregated form of Aβ (7A1a) (Figure 6). Upon visual inspection, aggregated Aβ appears to be more abundant in $A\beta_{1-42}$ NCs relative to $A\beta_{1-40}$. Quantification of the area of 7A1a staining, normalized to the area of neuronal marker Tuj1 to control for neuronal number indicates that $A\beta_{1-42}$ NCs contain about 4.8 times more aggregated Aβ peptide when compared to unedited H9 NCs and about 1.8 times more than $A\beta_{1-40}$ NCs (Figure 6). Statistical analysis of the average of 7A1a area in NCs of each genotype reveals that the increased aggregation of Aβ is statistically significant (H9 vs $A\beta_{1-42}$ P=0.0001 and $A\beta_{1-40}$ vs $A\beta_{1-42}$ P=0.0422). In addition to having increased Aβ aggregation, the aggregated Aβ also appears to localize near fragmented nuclei with especially bright fluorescence (Figure 7).

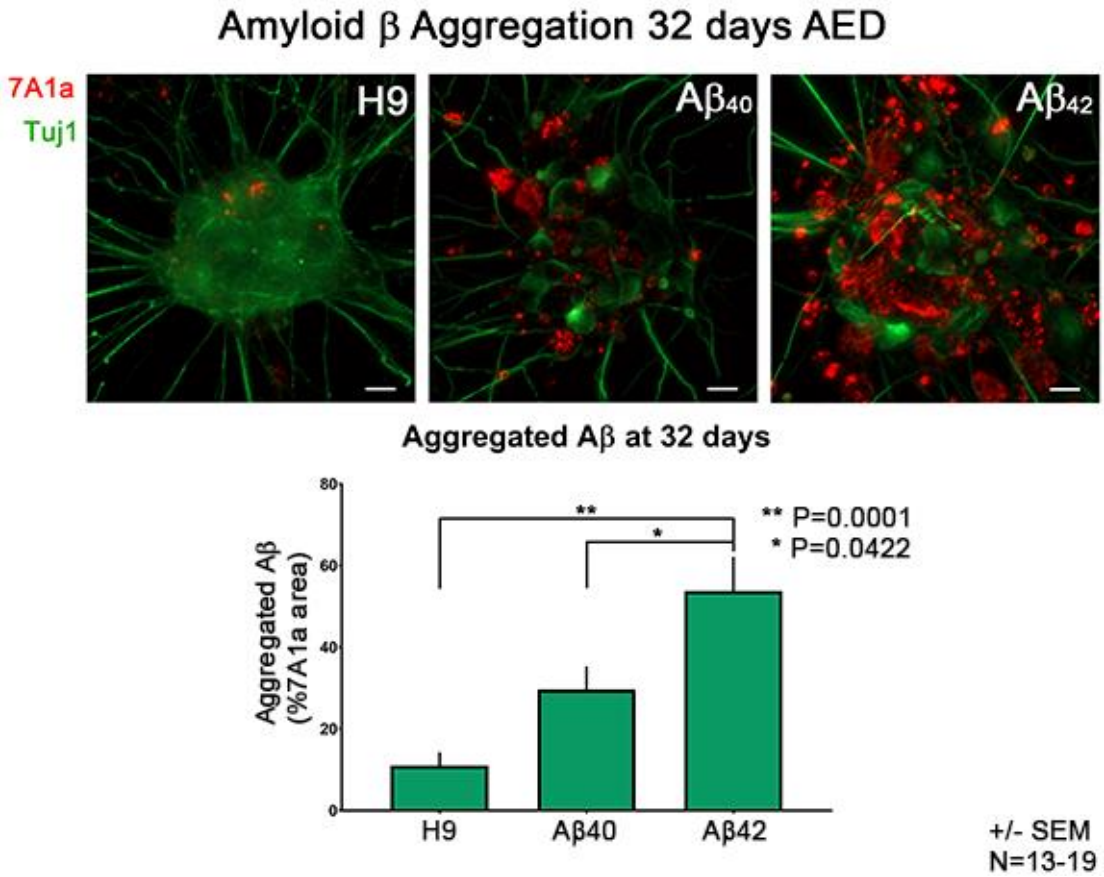

Figure 6. Aβ Aggregation in Neuronal Clusters 32 Days AED.
NCs were immunocytochemically stained with an antibody specific for aggregated Aβ (7A1a). Upon visual comparison, Aβ1-42 NCs clearly contain significantly more aggregated Aβ1-42 than either H9 or Aβ1-40 (top). When these images are quantified and normalized to the amount of Tuj1 present (a neuronal marker), Aβ1-42 NCs contain 54%, Aβ1-40 30%, and finally H9 NCs average 11%. Statistical analysis of average percentages of 7A1a shows a significant difference between H9 and Aβ1-42 (P=0.0001) and H9 vs Aβ1-40 (P=0.0422). Scale bar 10μm.

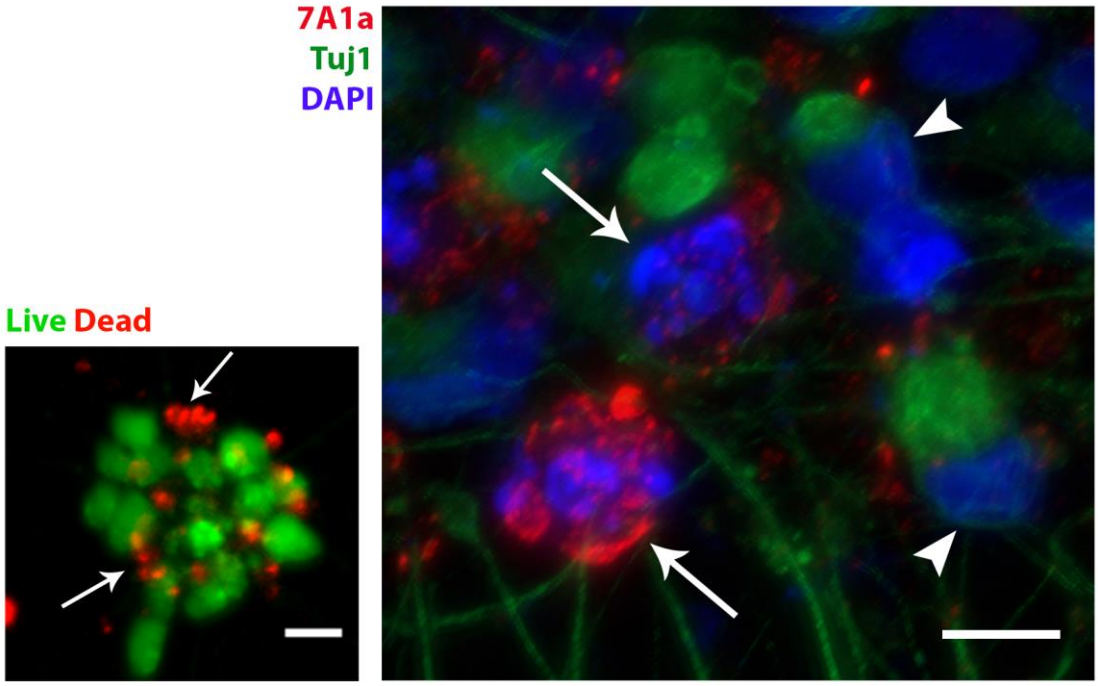

Figure 7. Aβ Aggregation is Localized Near Fractured Nuclei.
7A1a staining at 34 days AED shows that aggregated Aβ is heavily localized around fractured nuclei (arrows, right image) and the nuclei of neurons with very little staining (arrow heads, right image) do not have this fractured appearance. The live/dead assays at 34 days AED show that these neurons with fragmented nuclei are likely to be dead and/or dying (left image, arrows). Scale bars 10µm.

Synapse Decrease

A decrease in synapses is an early stage cellular phenotype which has been well documented in AD and thought to be associated with mild cognitive deficits that appear in individuals long before more severe symptoms. I used immunocytochemistry to measure synapsin1 puncta as an index of synapses. Synapsin1 stains a protein present in synaptic vesicles. Individual vesicles are

below the resolution limit of light microscopy, but cluster in groups at neuronal synapses. Image analysis revealed a statistically significant 2.8-fold decrease in the number synapses present in $A\beta_{1-42}$ neurons compared to H9 neurons (Figure 8).

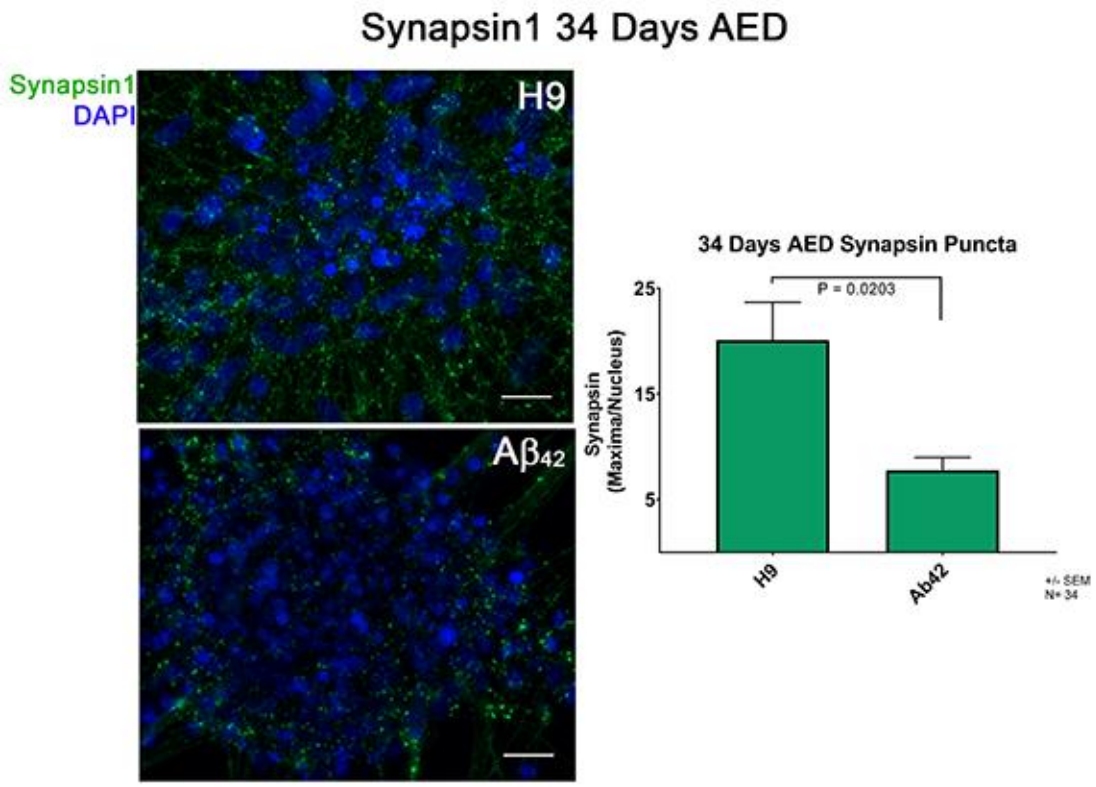

Figure 8. $A\beta_{1-42}$ Neurons Have Significantly Decreased Synapsin1 Puncta. Left, MIP of 0.5µm sections taken of H9 and $A\beta_{1-42}$ NCs. H9 NCs averaged 27.3 synapsin1 maxima/nucleus and $A\beta_{1-42}$ NCs 9.9 maxima/nucleus (P=0.0203). Scale bar 20µm.

Neurodegeneration

The later stages of AD are marked with increasing neuronal death in affected brain regions. A live/dead assay was used to estimate this phenotype in cultured cells at 10, 34, or 70 days AED (Figure 9). The method uses two fluorescent dyes to distinguish between live and dead cells: ethidium homodimer and calcein AM and is performed by incubating live neuronal cultures with a mixture of the indicators. Calcein AM is readily taken up by live cells but only fluoresces green when cleaved by cellular esterases which are not present in dead cells. Ethidium homodimer is live cell membrane impermeable but will fluoresce red when bound to DNA in dead cells with compromised plasma/nuclear membranes. At 34 days AED, there is no significant difference in cell death among the three genotypes. When the live/dead assay is repeated at 70 days AED, there is a large increase in cell death for both $A\beta_{1-40}$ and $A\beta_{1-42}$ genotypes relative to H9 parental cells (Figure 9). There is 2.3 times more cell death in $A\beta_{1-42}$ NCs over H9 and about 2 times more death in $A\beta_{1-40}$ NCs. To my knowledge this is the first mammalian experimental model that clearly exhibits a chronic progressive Aβ–dependent neurodegeneration phenotype and could thus be used to understand the mechanism of this process in human neurons.

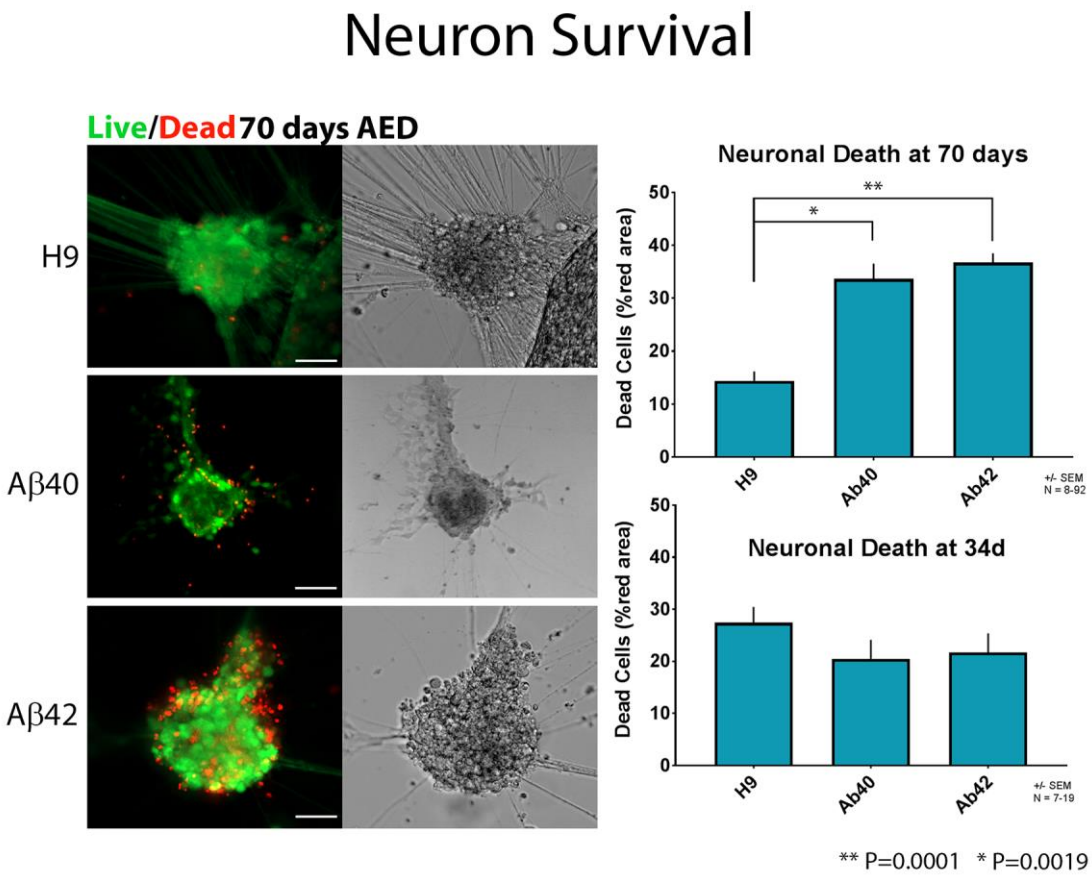

Figure 9. Neuron Survival at 34 and 70 Days AED.
A live/dead assay using calcein AM and ethidium homodimer was done on neurons at 34 days and 70 days AED. At 70 days AED $A\beta_{1-42}$ NCs begin to take on a granulated appearance and the number of axonal projections is reduced (left, brightfield images). Neuron death was quantified by calculating the percentage of red (dead) area of each NC. There is no difference in cell death between genotypes at 34 days AED. At 70 days AED, H9 NCs average 16%, $A\beta_{1-40}$ 33%, and $A\beta_{1-42}$ 38% red area. ANOVA with Dunnett's multiple comparisons test reveals that the increase in cell death is significant (H9 vs $A\beta_{1-40}$ P=0.0019 and H9 vs $A\beta_{1-42}$ P=0.0001, N=7-92). Scale bar 50µm.

Changes in Gene Expression and Pathway Analysis

Since my cells are isogenic, except for the edited alleles, they may be a good system to analyze the changes in gene expression that are dependent on direct expression of $A\beta_{1-42}$ or $A\beta_{1-42}$. mRNA was isolated from 34 day old neurons from multiple independently isolated clones of each genotype and characterized using RNA sequencing analysis. This provides data for the whole transcriptome rather than focusing on a preconceived hypothesized gene as is common in PCR based analyses. The differential gene expression (i.e. comparisons among samples with different genotypes) can provide unbiased clues to genes and pathways that are perturbed because of peptide expression and identify specific genes that could be targeted for therapeutic development and mechanistic analysis.

Clustering of expression changes in multiple samples of different genotypes shows that $A\beta_{1-42}$ clones group together and therefore have a similar expression pattern (Figure 10). Clustering of $A\beta_{1-40}$ and H9 genotypes are interspersed suggesting that they have more similar expression patterns to each other than to the $A\beta_{1-42}$ samples (Figure 10).

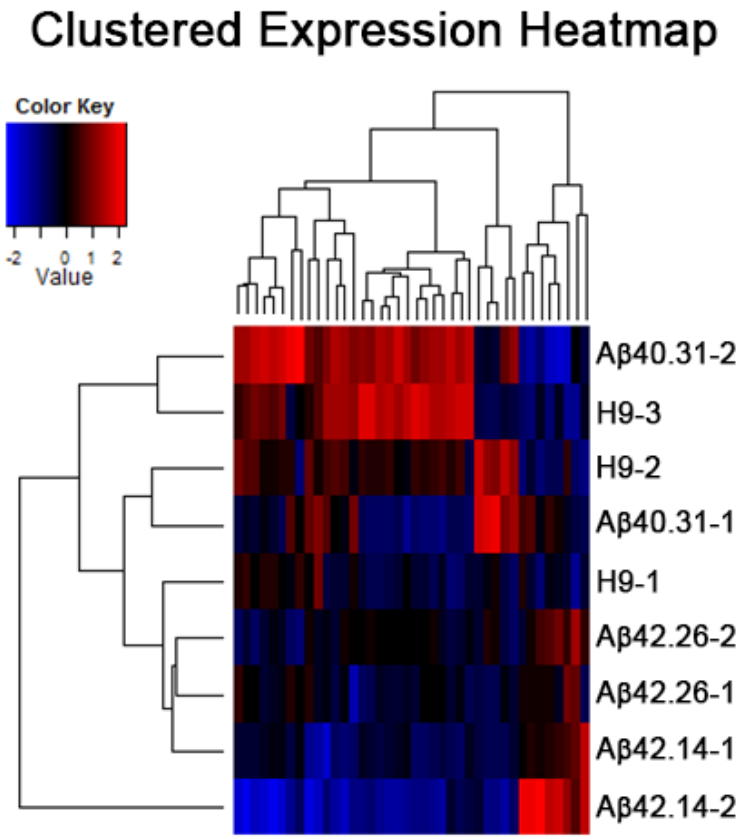

Figure 10. Heatmap of Changes in Gene Expression. Gene expression of 34 day AED neurons was centered on the median per batch prior to clustering. Results indicate that quantitative gene expression determined by RNA-seq analysis groups the $A\beta_{1-42}$ samples together (i.e. they are similar to each other, relative to the $A\beta_{1-40}$ or H9 genotypes). Note also that independently isolated clones cluster together. The data for H9 and $A\beta_{1-40}$ indicates that individual samples are interspersed with each other with respect to gene expression. This is consistent with $A\beta_{1-42}$ having different phenotypes relative to either $A\beta_{1-40}$ or H9.

Specific differentially expressed genes can be identified by plotting their expression p-values against their fold change. This results in a volcano plot

(when using the negative log of the p-values) allowing genes of high probability and high magnitude of change (either up or down regulated) to be easily visualized (Figure 11). When the top genes with changes in expression of both $A\beta_{1-40}$ vs H9 and $A\beta_{1-42}$ vs H9 are plotted together, there are some changes in expression that appear in both genotypes (Figure 12). This suggests that some differentially expressed genes in my edited cells (compared to unedited cells) may be due to the editing of one *App* allele rather than the expression of Aβ peptide. Changes seen in $A\beta_{1-42}$ but not in $A\beta_{1-40}$ are most likely to be $A\beta_{1-42}$ specific.

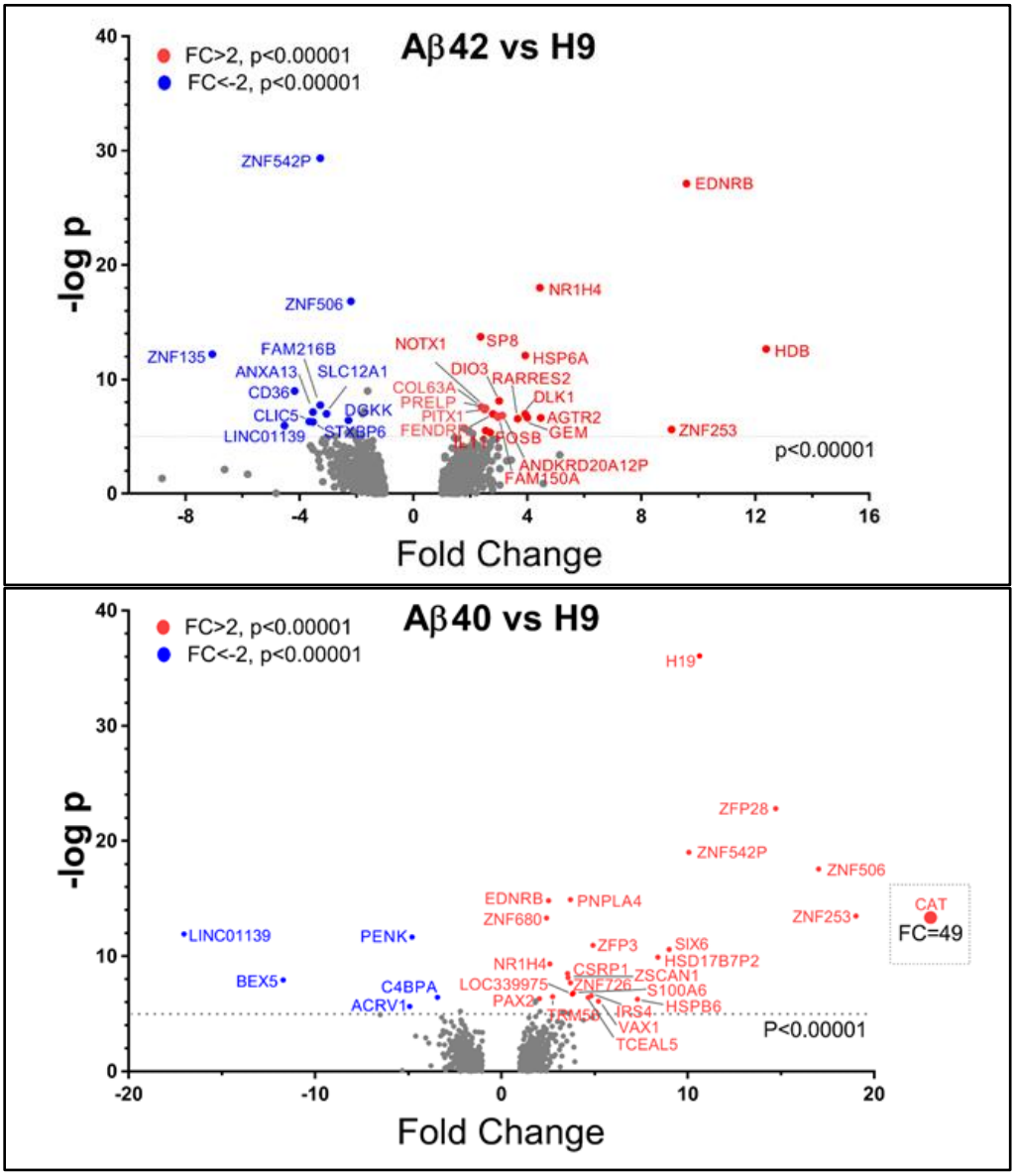

Figure 11. Volcano Plots of Differentially Expressed Genes at 34 Days AED.

Fold changes in gene expression were plotted as a function of their -log(p-value) (i.e. the absolute value of their significance). Only expression changes $2 > FC < -2$ and p<0.00001 are labeled in red (up regulated) or blue (down regulated.

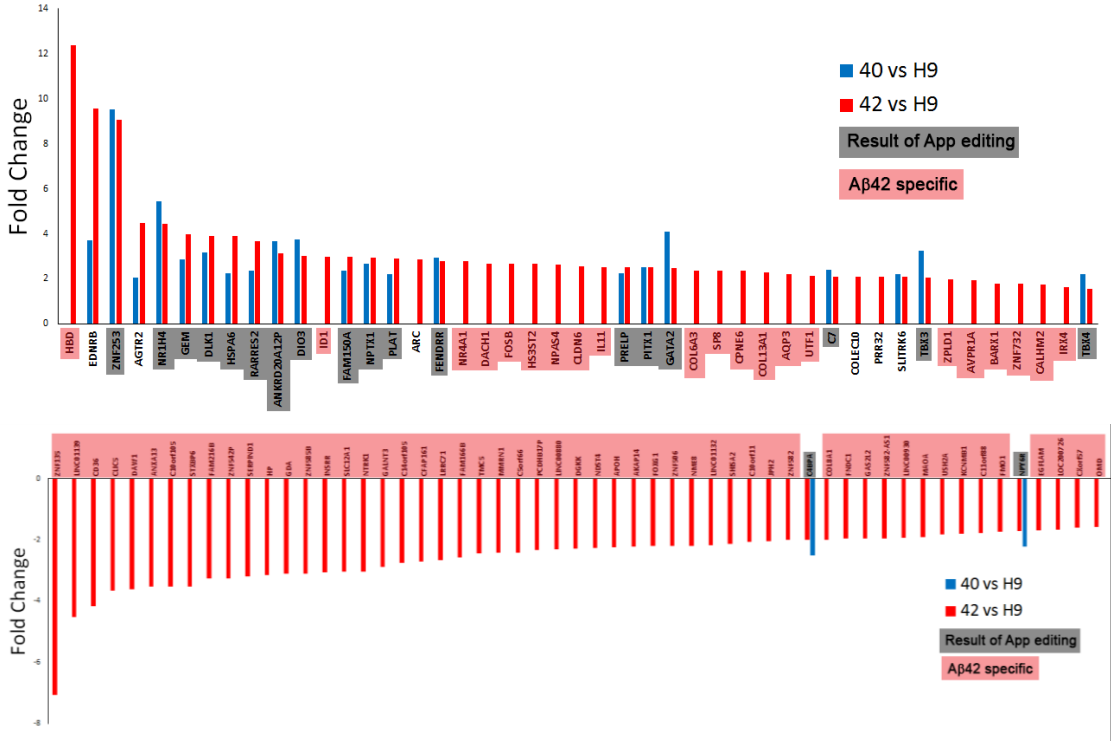

Figure 12. Some Changes in Expression Are Likely Due to *App E*diting. The highest upregulated (top) and downregulated (bottom) genes of $A\beta_{1\text{-}40}$ vs H9 and $A\beta_{1\text{-}42}$ vs H9 at 34 days AED. Some changes in expression occur in both the $A\beta_{1\text{-}40}$ and $A\beta_{1\text{-}42}$ genotypes and may thus be due to editing of one *App* allele (highlighted in grey). Changes in expression that do not appear in $A\beta_{1\text{-}40}$ are most likely to be $A\beta_{1\text{-}42}$ dependent (highlighted in red).

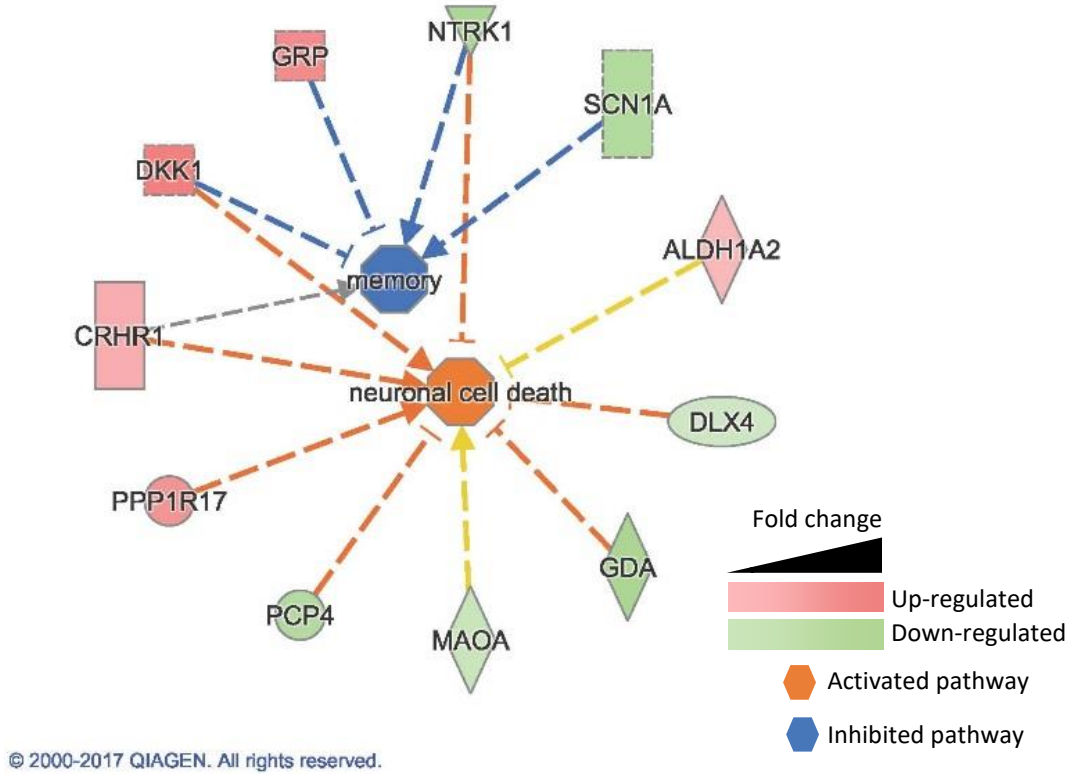

Figure 13. IPA Analysis of RNA Sequencing Data.
Ingenuity Pathway Analysis software was used to predict disease and function changes associated with differential gene expression of $A\beta_{1\text{-}42}$ compared to H9. The two categories with the highest z-score were memory (z=-1.980) and neuronal cell death (z=1.658) and are depicted. Genes that are upregulated appear in shades of red and downregulated genes appear in green with the darker shades indicating a higher fold change in expression. The memory pathway appears in blue, indicating that the expression profile of $A\beta_{1\text{-}42}$ neurons is likely to be inhibiting memory function. Neuronal cell death appears in orange, indicating that neuronal cell death pathways are likely to be activated. Remarkably, both of these phenotypes are key features of AD.

I also performed pathway analysis using Ingenuity software, a server based biological ontology. Remarkably the $A\beta_{1-42}$ vs H9 differential gene expression comparison revealed the two highest scoring (z-score, statistically normalized fold changes) for two functional/disease pathways: memory and neuronal cell death. These are the likely first and later stage phenotypes of AD. Figure 13 shows the pathways in a network diagram where individual genes are color coded relative to their differential expression and the arrows indicate predicted increases or decreases in the function/disease. In addition to these two pathways, there is also differential expression in several other genes associated with other pathways relevant to AD (Figure 14).

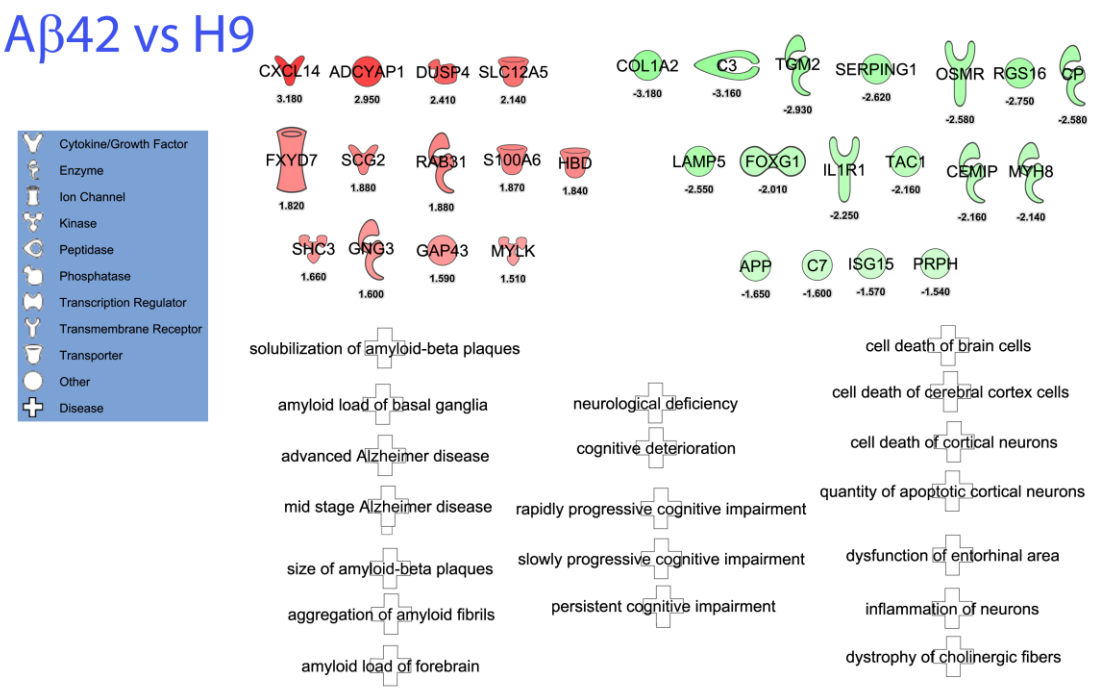

Figure 14. Differentially Expressed Genes Relevant to AD.
RNA sequencing data of $A\beta_{1\text{-}42}$ vs H9 differential expression of genes at 34 days AED related to AD. The shapes of differentially expressed genes correspond to their known functions and the darker shades correspond to higher fold changes. Under each gene is the fold-change found in RNA sequencing data. Pathways listed at the bottom are all AD related and are associated with changes in the genes listed. The $A\beta_{1\text{-}42}$ genotype shows expression changes of several genes in pathways related to AD.

CHAPTER FOUR

SUMMARY AND DISCUSSION

The genomic editing of my hESCs did not affect their ability to successfully differentiate into neurons. I measured the number of neurons present shortly after differentiation and found no difference between edited and unedited cell lines. After finding no differences in the number of neurons that develop, I followed and measured them as they aged. Up to 34 days, NCs appear similar in morphology and size. This was supported by the fact that when their area is measured, they are similar in size and increase similarly in size as they age.

$A\beta_{1-42}$ neurons have fewer synapsin1 puncta 32 days AED. Decreases in synapsin1 vesicles is an early and well-known cellular phenotype of AD. A decrease in the presence of synapsin1 has been previously shown to also coincide with dysfunction in the synaptic vesicle recycling pathway (Bogen et al., 2006).

The neurons in the $A\beta_{1-42}$ line accumulate significantly more aggregated Aβ than either H9 or $A\beta_{1-40}$ 34 days AED. $A\beta_{1-42}$ and $A\beta_{1-40}$ neurons also experience nearly triple the amount of cell death as H9 70 days AED. This is consistent with the fact that AD is a chronic and progressive disease. The $A\beta_{1-42}$ neurons accumulate aggregated Aβ long before neuronal death begins in the same way that amyloid plaques appear decades before symptoms in AD patients. This is also supportive of the hypothesis that Aβ is causative in AD.

There is much debate as to whether intracellular or extracellular aggregation of Aβ is toxic to neurons. Immunocytochemical staining of my $A\beta_{1-42}$ neurons supports the intracellular hypothesis. Because of the nature of cell culture, medium is replaced often and culture in 2D likely prevents Aβ from accumulating outside of neurons. In addition to this, immunocytochemical staining with 7A1a antibodies shows that aggregated Aβ accumulation is mainly located near fractured nuclei. From my live/dead assays, I also know that these cells are dead and/or dying.

RNA sequencing data of my neurons shows that independently isolated clones of each genotype cluster together and provides evidence that the phenotypes I see are not clone specific. There is also differential expression in several genes in pathways that are associated with AD, the most prominent of these being memory and neuronal cell death. When the most highly differentially expressed genes of $A\beta_{1-40}$ vs H9 and $A\beta_{1-42}$ vs H9 are compared, there is some overlap. These overlaps suggest that there may be some changes related to the editing of *App*.

This cellular model has advantages over other models in that it has direct expression so the time and uncertainty of factors required to generate $A\beta_{1-42}$ from APP are bypassed. Direct expression also eliminates the decades that is usually required for APP to be produced and accumulate within the brain, making this model suitable for a laboratory timescale. Since these cells are also isogenic the results obtained from this model are not confounded by the genetic variation that

often plagues iPSC and mouse models. This is supported by the fact that multiple independently isolated clones of each genotype show very limited differences. These cells are also heterozygous for ε4, an at-risk allele for AD.

One disadvantage of this model is that it requires a reliable neuronal differentiation protocol. There is variation in the differentiation of these cells and I have found that during differentiation there is sometimes a non-genotype specific failure of cells to survive the process. Other members of the lab also experience this non-genotype specific survival failure. Another potential drawback of this model is that there are solely neurons present in these cultures. Thus, it cannot address interactions with or issues related to the blood brain barrier as well as contributions by astrocytes or microglia.

While current and past models have provided researchers with answers about where Aβ comes from, how Aβ is processed from APP, and how Aβ aggregates, we still do not understand the mechanism behind how the neurons of AD affected patients are dying. Part of the reason for this is the lack of a model for AD that presents with clear AD phenotypes, namely neurodegeneration, as well as possible species differences between animal models and humans. This newly created model focuses on $A\beta_{1-42}$ dependent phenotypes and addresses both concerns by utilization of hESCs with direct expression of $A\beta_{1-42}$. By directly expressing $A\beta_{1-42}$ in human cells, this model also eliminates the time and uncertainty of factors required to generate $A\beta_{1-42}$ from APP as well as the decades that it usually takes to accumulate Aβ. I have demonstrated that these

edited stem cells can successfully differentiate into neurons without any significant abnormalities and later develop many of the characteristic neuropathologies of AD in culture. This is the first known model of $A\beta_{1-42}$ dependent ND in human neurons and could thus be used to identify therapeutic agents that slow or prevent this process and in addition may help elucidate the possible mechanisms behind neuronal death in AD.

CHAPTER FIVE

MATERIALS AND METHODS

Cell Culture and Maintenance

Cell Lines

WA09 H9 human embryonic stem cells were obtained from the WiCell Research Institute (Madison, WI, USA). TALEN editing was used to insert $A\beta_{1-42}$ or $A\beta_{1-40}$ sequence in the first exon of one APP allele. Cassette sequences can be found in Appendix A.

Stem Cell Maintenance

Stem cells were maintained on DR4 IRR mouse embryonic fibroblasts (MTI Global Stem; Gaithersburg, MD, USA) in HuES medium. HuES medium is Dulbecco's Modified Eagles Medium: nutrient mixture F-12 (DMEM/F12: Gibco), 20% KnockOut^{TM} Serum Replacement (Invitrogen), 50 U Penicillin and 50 mg/mL Streptomycin (Penicillin-Streptomycin, Gibco), 1% MEM Non-essential Amino Acids (Gibco), 1mM GlutaMax (Gibco), 0.1 mM β-Mercaptoethanol (Sigma), and 20ng/mL basic fibroblast growth factor (bFGF; Stemgent).

Neuronal Differentiation

Cells were differentiated according to a modified protocol based on a previously established protocol (Amoroso et al., 2013).

Embryoid body generation: On day zero, confluent wells of stem cells were passaged by incubation with Dispase (1mg/mL, Stem Cell Technologies) for 10-15 minutes. Cells were then washed twice with DPBS and triturated in 1mL of

PBS. Cells were then resuspended to $4x10^5$ cells/mL in HuES supplemented with 10µM Y-27632 (StemGent), 10µM SB-431542 (StemGent), 0.2µM LDN-193189 (StemGent) and plated in 10cm petri dishes coated with 6mL of 1.5% Agar (or ultra-low attachment dishes). Day two: Embryoid Bodies were collected into 50mL conical tubes, allowed to settle for 45 minutes, and as much media was removed from the cells before plating again in the same media as day zero. Day three: Collect embryoid bodies as on day two and change to Neural Induction Medium (NIM) supplemented with 20ng/mL bFGF, 10µM Y-27632, 10µM SB-431542, and 0.2µM LDN-193189. NIM is DMEM/F12, 50U Penicillin, 50mg/mL streptomycin, 1% Non-essential Amino Acids, 1mM Glutamax, 1x N-2 Supplement (Gibco), and 2µg/mL Heparin (Sigma-Aldrich). Day five: Collect cells as above and switch to NIM with 20ng/mL bFGF, 10µM SB-431542, 0.2µM LDN-193189, 10ng/mL brain-derived neurotrophic factor (BDNF, PreproTech), 0.4µg/mL Ascorbic Acid (AA, Sigma), 1µM Retinoic Acid (RA, Sigma). Day 7-15: Collect cells as above and use NIM supplemented with 10ng/mL BDNF, 0.4µg/mL AA, 1µM RA, 2µM Smoothened agonist (SAG, Calibochem). Change media every 2-3 days. Day 17+: Collect cells as above and switch to Neural Differentiation Medium (NDM) supplemented with 10ng/mL BDNF, 0.4µg/mL AA, 1µg/mL RA, 2µg/mL SAG, 1x B-27 supplement (Gibco), 10ng/mL glial cell line-derived neurotrophic factor (GDNF, PreproTech), 10ng/mL ciliary neurotrophic factor (CNTF, PreproTech), 10ng/mL insulin-like growth factor 1 (IGF-1,

PreproTech). Change media every 2-3 days. Dissociate EB bodies anytime between days 24 through 28.

Embryoid body dissociation: EBs are collected and rinsed in calcium and magnesium-free PBS (Corning Cell Grow). Then they were incubated with trypsin for 1-4 minutes. Then one equal volume fetal bovine serum (FBS, Hyclone) and two volumes of complete trituration wash medium (CTWM) are added. CTWM consists of calcium and magnesium free PBS, 25mM glucose (Mallinchrodt), 0.1% dialyzed bovine serum albumin (BSA, Roche), 1x N-2 supplement, 1x B-27 supplement, 2mM $MgCl_2$, 1mM ethylenediaminetetraacetic acid (EDTA, J.T. Baker), and 2.5% FBS. Centrifuge cells at 1400rpm for three minutes. Remove supernatant and re-suspend in 1mL of CTWM. Then triturate clumps with a p1000 pipette for seven passes. Add 10-12mL of CTWM and filter through a 40µm filter (Corning). Record volume and count cells. Centrifuge at 1400rpm for 4 minutes and resuspend cells in NDM supplemented with 1x B-27 supplement, 10ng/mL BDNF, 10ng/mL GDNF, 10ng/mL IGF-1, 10ng/mL CNTF, 0.4µg/mL AA, 25µM glutamate, 25µM β-mercaptoethanol, and 1mM RA. Seed cells at 1.5 - $1.8x10^6$ cells per well of a 6-well plate coated with laminin (company) and poly-ornithine (company). Laminin in DMEM/F12 (15µg/mL) is coated 48 hours prior to cell plating for 24 hours and poly-ornithine in DMEM/F12 (100µg/mL) is coated after for 24 hours prior to cell plating.

Neuron Maintenance

Neurons were maintained in NDM supplemented with 1x B-27 supplement, 10ng/mL BDNF, 10ng/mL GDNF, 10ng/mL IGF-1, 10ng/mL CNTF, 0.4µg/mL AA, 25µM glutamate, 25µM β-mercaptoethanol, and 1mM RA. Cultures were treated with 0.5µM ethynyl deoxyuridine (EdU) for 24 hours once a week, starting on the day of dissociation until day 50 post EB dissociation to maintain post-mitotic neurons only.

Quantitative Real-Time PCR

Total RNA extraction was done using RNeasy Micro Kit from (Qiagen) using the manufacturer's protocol. One well of a 6-well plate of healthy neurons usually yields approximately $1x10^6$ cells and 1-3µg of total RNA. RNA concentration and purity were determined using a NanoDrop ND-1000 Nanospectrophotometer (ThermoFisher Scientific). cDNA was prepared using qScript cDNA SuperMix (Quanta) following the manufacturers protocol. All qRT-PCR reactions were carried out in a 20µl reaction mixture containing 12.5µl iQTM SYBR® Green Supermix (Bio-Rad), 2µM of each forward and reverse primer, 0.25µg cDNA, and DEPC-Treated Water (Ambion) to adjust the final volume to 20µL. Amplification was carried out using a BioRad CFX96 TouchTM Real-Time PCR Detection System in clear 96 well sealed plates.

Cycling Conditions were as follows:

Initial denaturation/enzyme activation 95°C for 3 minutes

Denature: 95°C for 30 seconds

Annealing and Extension: 55°C for 20 seconds, 40 cycles

Melt Curve: 55°C to 95°C for 5 seconds in 0.5°C increments

Table 1. Quantitative Real-Time PCR Primers

Primer	Forward (5'→3')	Reverse (5'→3')
APP5*	GAGGAGGATGACTCGGATGTCTGG	GGTGGTTCTCTCTGTGGCTTCTTCGT
GAPDH	ATGGGGAAGGTGAAGGTCGGAGTC	GGGATTTCCATTGATGACAAGCTTCCCG
Aβ†	ATGGCGCAGTTCCTGAGA	ATGATTGCACCTTTGTTTGAACC

*App5 primer spans the junction between exons 5 and 6

† primer is the beginning of the secretory signal sequence (not found in the human genome)

Immunocytochemistry

Cells were grown on 15mm No.1 coverslips (FisherScientific) and incubated with freshly made 4% Paraformaldehyde for 20 minutes. Then, 4% Paraformaldehyde is removed and cells are washed with PBS for 5 minutes 3x. Coverslips were stored in 0.03%NaN_3 PBS at 4°C until use.

For Immunostaining, coverslips were incubated with blocking buffer (0.3% Triton X-100 and 5% Bovine Serum Albumin in PBS) for 45 minutes at room temperature. Blocking buffer is then removed, coverslips are briefly rinsed with PBS, and primary antibodies diluted in antibody buffer (0.3% Triton x-100 and 1% Bovine Serum Albumin in PBS) are added. Cells are incubated in primary antibodies overnight at 4°C. Primary antibodies are then removed and coverslips

are washed with PBS for 5 minutes 3x. Secondary antibodies are diluted with antibody buffer and are then added to the coverslips and incubated for two hours at room temperature protected from light. The secondary antibody solution is then removed and coverslips are washed again with PBS for 5 minutes 3x. Coverslips are then incubated with DAPI (1µg/µl) for 5 minutes at room temperature protected from light and washed with PBS for 5 minutes 2x. Coverslips were then mounted onto glass slides using Dako Fluorescent Mounting Medium. Fluorescent images were taken using the Zeiss Observer II microscope using either of the following objectives: 63X/1.4NA Plan-Apochromat DIC OIL or 20X/0.80NA Plan-Apochromat DIC and a Zeiss AxioCam 506. ZEN Blue software was used to capture images.

Table 2. Antibodies Used for Immunocytochemistry

Antibody	Dilution	Supplier	Catalog No.
NeuN	2µg/mL	Abcam	Ab104224
Lamp1	0.25µg/mL	Abcam	Ab24170
DCX	1µg/mL	Abcam	Ab77450
Oligomeric Aβ (7A1a)	1.4µg/mL	New England Rare Reagents	N/A
Synapsin I	0.2µg/mL	Abcam	Ab8
Goat anti-Chicken IgY H&L (Alexa Flour 488)	3.9-3.98µg/mL	Abcam	Ab150169
Goat anti-Rabbit IgG H&L (Alexa Flour 488)	2µg/mL	Abcam	Ab150077
Goat anti-Mouse IgG H&L (Alexa Flour 594)	2µg/mL	Invitrogen	A11005

Image Analysis

All image handling and processing was done with Fiji image analysis software (Schindelin et al., 2012). NeuN and DCX positive cells were counted and normalized to the total number of DAPI stained nuclei present in the same field. NeuN and DAPI were both counted using the Otsu method in ImageJ and DCX positive cells were counted manually. Oligomeric Aβ (7A1a) quantification was done by creating a tightly bound box around each individual neuronal cluster and cropping the image to this area. Background was subtracted using a 150-pixel rolling ball radius. A maximum intensity projection was then created from an image stack (0.5μm Z intervals, 16-60 images), then using the Z-projection maximum intensity algorithm. The individual color channels were separated and the Aβ channel was thresholded using the IsoData method to measure the area of positive staining within the neural cluster and expressed as a percentage of the total cluster area. Neuronal cluster area was measured from Hoffman interference contrast images by using the freehand tool to manually trace the edges of clusters and using the measure area function.

Live/dead analysis was done by staining neuronal clusters growing on coverslips or in 12 well plates using ethidium homodimer (red fluorescence, dead cells) and calcein AM esterase substrate (green fluorescence when hydrolyzed). Three to five individual focal planes were obtained as well as a reference Hoffman interference contrast image. The number of pixels in an area was measured by separating individual color channels of the stack, subtracting

background using a 50-pixel rolling ball radius and creating a maximum intensity projection using auto brightness and contrast to threshold each channel. Data is presented as percent red area relative to the total area of red plus green channels.

Synapsin1 puncta quantification was done by subtracting the background using a 150-pixel rolling ball radius and creating a maximum intensity projection of a stack of images (0.5µm sections, 11-31 images). The nuclei were counted the same way as in the DCX and NeuN analysis and the synpasin1 puncta were counted using the ImageJ find maxima function. The number of synapsin1 puncta were then normalized to the number of DAPI nuclei present in each NC.

Brightfield Imaging

Brightfield Hoffman Modulated Contrast (HMC) images were taken using a Nikon Diaphot microscope using either of the following objectives: HMC EF 10X 0.25NA 160/- or HMC 20X LWD 0.4NA 160/0-2. A SPOT RT230 camera and SPOT Advanced software was used to capture images.

Statistical Analysis

All statistical analyses were done using at least three biological replicates and more than one clone per edited genotype. Each differentiation from stem cell expansion to neuron is considered one biological replicate. GraphPad Prism 7 software was used for all statistical calculations.

APPENDIX A

INSERTED CASSETTE SEQUENCES USING TALEN

Creation of the cell lines used in this research were carried out previously by members of the Salvaterra lab using TALEN. The sequences of the inserts include an ATG start codon followed by the rat preproenkephin sequence, the $A\beta_{1-40}$ or $A\beta_{1-42}$ sequence ending with a stop codon, followed by a pgk promoter with a puromycin selection gene and polyA tail all inserted within the first exon of *App* (Figure 15).

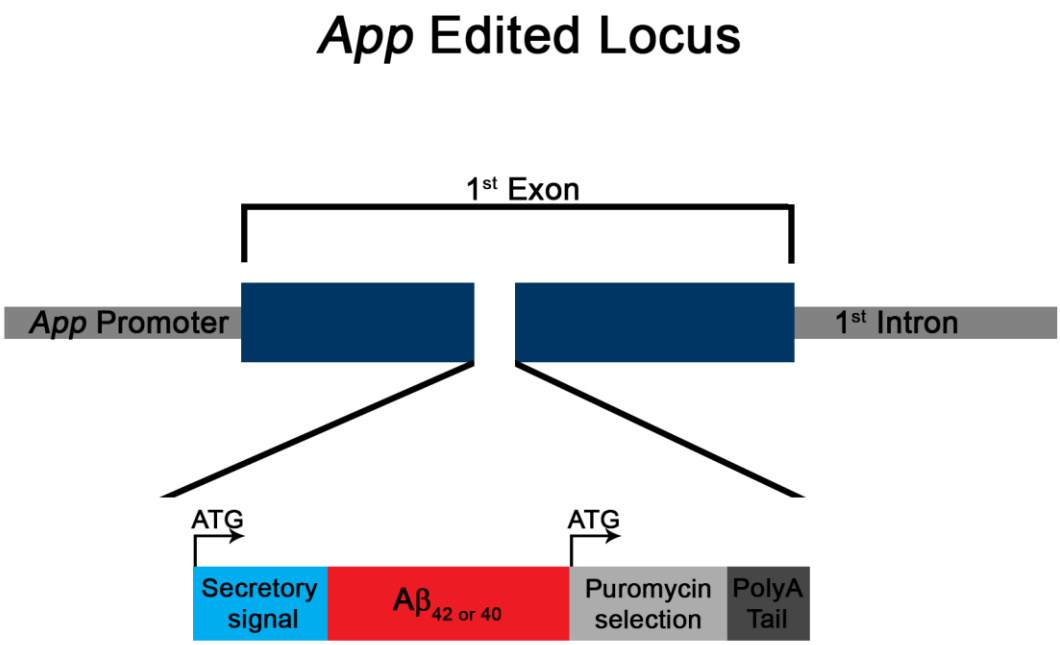

Diagram of edited *App* locus
The inserted cassette is within the first exon of *App*. The Cassette contains a start codon followed by a secretory sequence, the $A\beta_{1-42/40}$ sequence, puromycin selection, and finally a polyA tail.

APP exon 1, bases in red were cut out by TALENs:

```
GGATCAGCTG ACTCGCCTGG CTCTGAGCCC CGCCGCCGCG CTCGGGCTCC GTCAGTTTCC
TCGGCAGCGG TAGGCGAGAG CACGCGGAGG AGCGTGCGCG GGGGCCCCGG GAGACGGCGG
CGGTGGCGGC GCGGGCAGAG CAAGGACGCG GCGGATCCCA CTCGCACAGC AGCGCACTCG
GTGCCCCGCG CAGGGTCGCG ATGCTGCCCG GTTTGGCACT GCTCCTGCTG GCCGCCTGGA
CGGCTCGGGC GCTGGAG
```

Aβ$_{1-42}$ insert:

```
ATGGCGCAGT TCCTGAGACT TTGCATCTGG CTCGTAGCGC TTGGGTCCTG CCTCCTGGCT
ACAGTGCAGG CAGATGCAGA ATTCCGACAT GACTCAGGAT ATGAAGTTCA TCATCAAAAA
TTGGTGTTCT TTGCAGAAGA TGTGGGTTCA AACAAAGGTG CAATCATTGG ACTCATGGTG
GGCGGTGTTG TCATAGCGTAG
```

Aβ$_{1-40}$ insert:

```
ATGGCGCAGT TCCTGAGACT TTGCATCTGG CTCGTAGCGC TTGGGTCCTG CCTCCTGGCT
ACAGTGCAGG CAGATGCAGA ATTCCGACAT GACTCAGGAT ATGAAGTTCA TCATCAAAAA
TTGGTGTTCT TTGCAGAAGA TGTGGGTTCA AACAAAGGTG CAATCATTGG ACTCATGGTG
GGCGGTGTTG TCTAG
```

Pgk promoter with puro selection gene and poly A tail:

```
ATTCTACCGG GTAGGGGAGG CGCTTTTCCC AAGGCAGTCT GGAGCATGCG CTTTAGCAGC
CCCGCTGGGC ACTTGGCGCT ACACAAGTGG CCTCTGGCCT CGCACACATT CCACATCCAC
CGGTAGGCGC CAACCGGCTC CGTTCTTTGG TGGCCCCTTC GCGCCACCTT CTACTCCTCC
CCTAGTCAGG AAGTTCCCCC CCGCCCCGCA GCTCGCGTCG TGCAGGACGT GACAAATGGA
AGTAGCACGT CTCACTAGTC TCGTGCAGAT GGACAGCACC GCTGAGCAAT GGAAGCGGGT
AGGCCTTTGG GGCAGCGGCC AATAGCAGCT TTGCTCCTTC GCTTTCTGGG CTCAGAGGCT
GGGAAGGGGT GGGTCCGGGG GCGGGCTCAG GGGCGGGCTC AGGGGCGGGG CGGGCGCCCG
AAGGTCCTCC GGAGGCCCGG CATTCTGCAC GCTTCAAAAG CGCACGTCTG CCGCGCTGTT
CTCCTCTTCC TCATCTCCGG GCCTTTCGAC CTGCAGCCCA AGCTTACCAT GACCGAGTAC
AAGCCCACGG TGCGCCTCGC CACCCGCGAC GACGTCCCCA GGGCCGTACG CACCCTCGCC
GCCGCGTTCG CCGACTACCC CGCCACGCGC CACACCGTCG ATCCGGACCG CCACATCGAG
CGGGTCACCG AGCTGCAAGA ACTCTTCCTC ACGCGCGTCG GGCTCGACAT CGGCAAGGTG
TGGGTCGCGG ACGACGGCGC CGCGGTGGCG GTCTGGACCA CGCCGGAGAG CGTCGAAGCG
GGGGCGGTGT TCGCCGAGAT CGGCCCGCGC ATGGCCGAGT TGAGCGGTTC CCGGCTGGCC
GCGCAGCAAC AGATGGAAGG CCTCCTGGCG CCGCACCGGC CCAAGGAGCC CGCGTGGTTC
CTGGCCACCG TCGGCGTCTC GCCCGACCAC CAGGGCAAGG GTCTGGGCAG CGCCGTCGTG
CTCCCCGGAG TGGAGGCGGC CGAGCGCGCC GGGGTGCCCG CCTTCCTGGA GACCTCCGCG
CCCCGCAACC TCCCCTTCTA CGAGCGGCTC GGCTTCACCG TCACCGCCGA CGTCGAGGTG
CCCGAAGGAC CGCGCACCTG GTGCATGACC CGCAAGCCCG GTGCCTGAAT CCGTCGAGGA
ATTCACTCCT CAGGTGCAGG CTGCCTATCA GAAGGTGGTG GCTGGTGTGG CCAATGCCCT
GGCTCACAAA TACCACTGAG ATCTTTTTCC CTCTGCCAAA AATTATGGGG ACATCATGAA
GCCCCTTGAG CATCTGACTT CTGGCTAATA AAGGAAATTT ATTTTCATTG CAATAGTGTG
TTGGAATTTT TTGTGTCTCT CACTCGGAAG GACATATGGG AGGGCAAATC ATTTAAAACA
TCAGAATGAG TATTTGGTTT AGAGTTTGGC AACATATGCC CATATGCTGG CTGCCATG
```

APPENDIX B

RNA SEQUENCING DATA

RNA Sequencing data of $A\beta_{1-42}$ vs H9

Table includes differentially expressed genes with a fold change = |1.5| and a false discovery rate <0.05.

ID	Fold Change (FC)	p-value	False Discovery Rate (q)
AGTR2	4.47	0.000000238	0.000167
ANKRD20A12P	3.12	0.000000142	0.000118
AQP3	2.22	0.000103	0.023
ARC	2.85	0.0000172	0.00583
AVPR1A	1.95	0.00000309	0.00161
BARX1	1.79	0.00023	0.0415
C7	2.11	0.000189	0.0363
CALHM2	1.74	0.0000722	0.018
CLDN6	2.57	0.000179	0.0352
COL13A1	2.28	0.0000655	0.0169
COL6A3	2.38	2.55E-08	0.0000359
COLEC10	2.11	0.0000285	0.00883
CPNE6	2.35	0.0000956	0.0218
DACH1	2.69	0.0000704	0.0179
DIO3	3.01	7.57E-09	0.0000126
DLK1	3.92	0.000000105	0.0000927
EDNRB	9.58	7.63E-28	6.97E-24
FAM150A	2.97	0.000000209	0.000159
FENDRR	2.79	0.000000107	0.0000927
FOSB	2.69	0.00000439	0.00216
GATA2	2.46	0.0000176	0.00583
GEM	4	0.000000224	0.000164
HBD	12.38	2.23E-13	6.79E-10
HS3ST2	2.69	0.0000365	0.0106
HSPA6	3.92	8.1E-13	1.85E-09
ID1	2.99	0.0000923	0.0216
IL11	2.53	0.00000297	0.0016
IRX4	1.64	0.000132	0.0283
NPAS4	2.62	0.000121	0.0264
NPTX1	2.95	0.000000166	0.000132
NR1H4	4.44	9.74E-19	5.93E-15
NR4A1	2.79	0.0000173	0.00583
PITX1	2.5	4.51E-08	0.0000549
PLAT	2.91	0.0000164	0.00583
PRELP	2.53	3.31E-08	0.0000432
PRR32	2.08	0.00006	0.0159

RARRES2	3.66	0.000000278	0.000188
SLITRK6	2.08	0.00000549	0.00257
SP8	2.36	1.89E-14	6.92E-11
TBX3	2.07	0.000187	0.0363
TBX4	1.55	0.000203	0.0382
UTF1	2.13	0.0000345	0.0102
ZNF253	9.06	0.00000246	0.00136
ZNF732	1.78	0.00000195	0.00111
ZPLD1	1.97	0.0000787	0.0192
AKAP14	-2.23	0.000286	0.0497
ANXA13	-3.53	7.15E-08	0.0000768
APOH	-2.25	0.000105	0.0231
C10orf105	-3.53	0.000136	0.0288
C10orf11	-2.06	0.000169	0.0339
C11orf88	-1.78	0.000285	0.0497
C14orf105	-2.75	0.00000924	0.00401
C4BPA	-2	0.0000202	0.00658
C5orf66	-2.41	0.0000941	0.0218
CD36	-4.17	1.03E-09	0.00000194
CFAP161	-2.71	0.0000425	0.0119
CLIC5	-3.66	0.000000493	0.00031
COL8A1	-1.99	0.0000119	0.00488
CXorf57	-1.61	1.06E-09	0.00000194
DAW1	-3.61	0.0000657	0.0169
DGKK	-2.28	0.000000382	0.000249
EGFLAM	-1.68	0.000156	0.0317
FAM166B	-2.57	0.000254	0.0455
FAM216B	-3.27	1.79E-08	0.0000273
FMO1	-1.73	5.92E-08	0.0000676
FNDC1	-1.95	0.000156	0.0317
FOXG1	-2.2	0.00000694	0.00317
GALNT3	-2.89	0.000154	0.0317
GAS2L2	-1.95	0.000209	0.0386
GDA	-3.1	0.0000447	0.0123
HP	-3.16	0.0000172	0.00583
INSRR	-3.07	0.000014	0.00526
JPH2	-2.04	0.00000921	0.00401
KCNMB1	-1.79	0.000000102	0.0000927
LINC00880	-2.3	0.00000493	0.00237
LINC00930	-1.93	0.0000451	0.0123
LINC01132	-2.17	0.000141	0.0295

LINC01139	-4.53	0.00000112	0.00066
LOC200726	-1.67	0.0000386	0.011
LRRC71	-2.66	0.0000492	0.0132
MAOA	-1.92	0.0000141	0.00526
MMRN1	-2.43	0.000207	0.0386
NDST4	-2.27	0.000259	0.0459
NME8	-2.19	0.000229	0.0415
NPY6R	-1.72	0.0000847	0.0204
NTRK1	-3.03	0.0000125	0.00488
OMD	-1.58	0.0000309	0.00941
PCDHB17P	-2.33	0.000179	0.0352
SERPIND1	-3.2	0.0000315	0.00941
SHISA2	-2.14	0.00000323	0.00164
SLC12A1	-3.05	0.000000104	0.0000927
STXBP6	-3.53	0.000000536	0.000326
TMC5	-2.45	0.0000729	0.018
USH2A	-1.83	0.0000103	0.00437
ZNF135	-7.06	6.4E-13	1.67E-09
ZNF506	-2.2	1.47E-17	6.72E-14
ZNF542P	-3.27	4.62E-30	8.43E-26
ZNF582	-2.01	0.0000122	0.00488
ZNF582-AS1	-1.95	0.0000224	0.00718
ZNF585B	-3.1	0.000201	0.0382

RNA Sequencing data of $A\beta_{1\text{-}40}$ vs H9

Table includes differentially expressed genes with a fold change $= |1.5|$ and a false discovery rate <0.05.

ID	Fold Change(FC)	p-value	False Discovery Rate (q)
AGTR2	2.04	0.0000353	0.0143
ANGPTL1	2.23	0.0000946	0.032
ANKRD20A12P	3.68	4.11E-09	0.00000683
AVPR1A	2	0.0000317	0.0135
C7	2.39	0.0000402	0.016
CALB1	2.17	0.000144	0.0425
COL6A3	5.66	1.39E-08	0.0000169
CSRP1	3.14	1.38E-09	0.00000315
CXorf57	3.48	4.38E-11	0.000000133
DIO3	3.76	0.00000177	0.00108
DLK1	3.18	0.00009	0.031

DNAJA4	2.93	0.00000264	0.00155
EDNRB	3.71	2.9E-21	1.77E-17
FAM150A	2.38	0.000143	0.0425
FENDRR	2.93	1.12E-08	0.0000158
GATA2	4.11	0.00000133	0.000837
GDF10	2.73	0.000000176	0.000146
GEM	2.85	0.0000706	0.0253
GFAP	2.17	0.000000551	0.000373
H19	71.51	8.06E-58	1.47E-53
HSPA6	2.25	0.00000581	0.00312
IRS4	4.03	0.000000485	0.00034
LGR5	1.62	0.0000537	0.02
PRODH	2.41	0.000111	0.0363
LRRC61	2.25	4.77E-08	0.0000484
NPTX1	2.69	0.0000268	0.012
NR1H4	5.46	7.9E-17	2.88E-13
PAX2	2.48	1.74E-08	0.0000199
PITX1	2.51	6.67E-08	0.0000641
PLAT	2.22	0.0000516	0.0196
PNPLA4	7.62	7.79E-24	7.11E-20
POTEM	2.1	0.0000681	0.0249
POU4F1	2	0.000111	0.0363
PRELP	2.25	0.00000348	0.00198
RARRES2	2.38	0.00000124	0.000807
S100A6	4.53	3.34E-09	0.00000609
SERPINE1	3.76	0.0000311	0.0135
SIX6	6.77	0.000000339	0.000247
SLC14A1	1.64	0.0000432	0.0168
SLITRK6	2.19	0.0000214	0.0103
SST	1.75	0.000135	0.0417
SYT10	2.71	0.0000242	0.0113
TBX3	3.25	0.0000726	0.0255
TBX4	2.22	0.00000033	0.000247
TCEAL5	4.03	0.000000281	0.000223
TNFRSF11B	3.07	0.0000047	0.0026
TRIM58	3.56	1.32E-08	0.0000169
VAMP5	4.14	0.000141	0.0425
ZFP3	4.56	8.63E-09	0.0000131
ZIC4	1.96	0.000116	0.0368
ZNF253	9.51	0.0000165	0.00835
ZNF595	2.58	0.00000976	0.00509

ZNF680	3.78	7.43E-21	3.39E-17
ZNF790-AS1	2.71	5.76E-11	0.00000015
ZSCAN1	3.32	0.000000111	0.0000965
BEX5	-10.7	8.26E-08	0.0000754
C4BPA	-2.5	0.0000348	0.0143
LINC01139	-9.92	3.21E-09	0.00000609
LINC01146	-3.66	0.000117	0.0368
MLC1	1.44	0.0000253	0.0116
NPY6R	-2.22	0.0000204	0.01
PENK	-2.83	3.21E-08	0.0000345

REFERENCES

Abramowski, D., Rabe, S., Upadhaya, A. R., Reichwald, J., Danner, S., Staab, D., Staufenbiel, M. (2012). Transgenic Expression of Intraneuronal Aβ42 But Not Aβ 40 Leads to Cellular Aβ Lesions, Degeneration, and Functional Impairment without Typical Alzheimer's Disease Pathology. *Journal of Neuroscience*, *32*(4), 1273–1283. https://doi.org/10.1523/JNEUROSCI.4586-11.2012

Alzforum. (2016). Research Models, 1–9. Retrieved from http://www.alzforum.org/research-models

Amoroso, M. W., Croft, G. F., Williams, D. J., Keeffe, S. O., Carrasco, M. A., Davis, A. R., Wichterle, H. (2013). Accelerated high-yield generation of limb-innervating motor neurons from human stem cells. *Journal of Neuroscience*, *33*(2), 574–586. https://doi.org/10.1523/JNEUROSCI.0906-12.2013.Accelerated

Bales, K. R. (2012). The value and limitations of transgenic mouse models used in drug discovery for Alzheimer's disease: an update. *Expert Opinion on Drug Discovery*. https://doi.org/10.1517/17460441.2012.666234

Ballatore, C., Lee, V., & J, T. (2007). Tau-mediated neurodegeneration in Alzheimer's disease and related disorders. *Nature Reviews. Neuroscience*, *8*(9), 663–672. https://doi.org/10.1038/nrn2194

Ballatore, C., Lee, V. M.-Y., & Trojanowski, J. Q. (2007). Tau-mediated neurodegeneration in Alzheimer's disease and related disorders. *Nature*

Reviews. Neuroscience, *8*(9), 663–72. https://doi.org/10.1038/nrn2194

Bertram, L., Lill, C. M., & Tanzi, R. E. (2010). The genetics of alzheimer's disease: Back to the future. *Neuron*, *68*(2), 270–281. https://doi.org/10.1016/j.neuron.2010.10.013

Bogen, I. L., Boulland, J., Mariussen, E., Wright, M. S., Fonnum, F., Kao, H., & Walaas, S. I. (2006). Absence of synapsin I and II is accompanied by decreases in vesicular transport of specific neurotransmitters, 1458–1466. https://doi.org/10.1111/j.1471-4159.2005.03636.x

Castano, E. M., Prelli, F., Wisniewski, T., Golabek, A., Kumar, R. A., Soto, C., & Frangione, B. (1995). Fibrillogenesis In Alzheimers Disease Of Amyloid β Peptides and Apolipoprotein E. *Biochemical Journal*, *306*(Part 2), 599–604.

Choy, R. W.-Y., Cheng, Z., & Schekman, R. (2012). Amyloid precursor protein (APP) traffics from the cell surface via endosomes for amyloid β (Aβ) production in the trans-Golgi network. *Proceedings of the National Academy of Sciences of the United States of America*, *109*(30), E2077-82. https://doi.org/10.1073/pnas.1208635109

Cowan, C. M., Shepherd, D., & Mudher, A. (2010). Insights from *Drosophila* models of Alzheimer's disease. *Biochemical Society Transactions*, *38*(4), 988–992. https://doi.org/10.1042/BST0380988

Farrer, L. A., Cupples, A. L., Kukull, W. a, Mayeux, R., Myers, R. H., Pericak-vance, M. a, van Duijn, C. M. (1997). Effects of Age, Sex, and Ethnicity on the Association Between Apolipoprotein E Genotype and Alzheimer

Disease. *JAMA: The Journal of the American Medical Association*, *278*, 1349–1356. https://doi.org/10.1001/jama.1997.03550160069041

FastStats - Leading Causes of Death. (2016). Retrieved January 1, 2016, from http://www.cdc.gov/nchs/fastats/leading-causes-of-death.htm

Funk, W. D., Labat, I., Sampathkumar, J., Gourraud, P. A., Oksenberg, J. R., Rosler, E., West, M. D. (2012). Evaluating the genomic and sequence integrity of human ES cell lines; comparison to normal genomes. *Stem Cell Research*, *8*(2), 154–164. https://doi.org/10.1016/j.scr.2011.10.001

Götz, J., Schild, A., Hoerndli, F., & Pennanen, L. (2004). Amyloid-induced neurofibrillary tangle formation in Alzheimer's disease: Insight from transgenic mouse and tissue-culture models. *International Journal of Developmental Neuroscience*, *22*(7), 453–465. https://doi.org/10.1016/j.ijdevneu.2004.07.013

Gutierrez-Zepeda, A., & Luo, Y. (2004). Testing the amyloid toxicity hypothesis of Alzheimer's disease in transgenic Caenorhabditis elegans model. *Front Biosci*, *9*, 3333–3338. https://doi.org/1485 [pii]

Haass, C., Kaether, C., Thinakaran, G., & Sisodia, S. (2012). Trafficking and proteolytic processing of APP. *Cold Spring Harbor Perspectives in Medicine*, *2*(5), 1–25. https://doi.org/10.1101/cshperspect.a006270

Hartmann, T., Bieger, S. C., Bruhl, B., Tienari, P. J., Ida, N., Allsop, D., … Beyreuther, K. (1997). Distinct sites of intracellular production for Alzheimer's disease Aβ40/42 amyloid peptides. *Nature Medicine*, *3*(9),

1016–1020. https://doi.org/10.1038/nm0798-822

Hebert, L. E., Weuve, J., Scherr, P. A., & Evans, D. A. (2013). Alzheimer disease in the United States (2010-2050) estimated using the 2010 census. *Neurology*, *80*(19), 1778–1783. https://doi.org/10.1212/WNL.0b013e31828726f5

Hu, X., Crick, S. L., Bu, G., Frieden, C., Pappu, R. V, & Lee, J.-M. (2009). Amyloid seeds formed by cellular uptake, concentration, and aggregation of the amyloid-beta peptide. *Proceedings of the National Academy of Sciences of the United States of America*, *106*(48), 20324–9. https://doi.org/10.1073/pnas.0911281106

Ihara, Y., Morishima-Kawashima, M., & Nixon, R. (2012). The ubiquitin-proteasome system and the autophagic-lysosomal system in Alzheimer disease. *Cold Spring Harbor Perspectives in Medicine*, *2*(8). https://doi.org/10.1101/cshperspect.a006361

Iijima-Ando, K., Hearn, S. A., Shenton, C., Gatt, A., Zhao, L., & Iijima, K. (2009). Mitochondrial mislocalization underlies Aβ42-induced neuronal dysfunction in a drosophila model of alzheimer's disease. *PLoS ONE*, *4*(12). https://doi.org/10.1371/journal.pone.0008310

Iijima-Ando, K., & Iijima, K. (2009). Transgenic Drosophila models of Alzheimer's disease and tauopathies. *Brain Struct Funct*, *214*(2–3), 245–262.

Iijima-Ando, K., & Iijima, K. (2010). Transgenic drosophila models of Alzheimer's disease and tauopathies. *Brain Structure and Function*, *214*(2–3), 245–262.

https://doi.org/10.1007/s00429-009-0234-4

Kanekiyo, T., Xu, H., & Bu, G. (2014). ApoE and A?? in Alzheimer's disease: Accidental encounters or partners? *Neuron*, *81*(4), 740–754. https://doi.org/10.1016/j.neuron.2014.01.045

Kang, J., Lemaire, H.-G., Unterbeck, A., Salbaum, J. M., Masters, C. L., Grzeschik, K.-H., Muller-Hill, B. (1987). The precursor of Alzheimer's disease amyloid A4 protein resembles a cell-surface receptor. *Nature*, *325*(19), 733–736. https://doi.org/10.1038/325733a0

Kondo, T., Asai, M., Tsukita, K., Kutoku, Y., Ohsawa, Y., Sunada, Y., … Inoue, H. (2013). Modeling Alzheimer's disease with iPSCs reveals stress phenotypes associated with intracellular Aβ and differential drug responsiveness. *Cell Stem Cell*, *12*(4), 487–496. https://doi.org/10.1016/j.stem.2013.01.009

Kovacs, D. M., & Tanzi, R. E. (1998). Monogenic determinants of familial Alzheimer' s disease : presenilin-1 mutations, *54*, 902–909.

LaFerla, F. M. (2010). Pathways linking Abeta and tau pathologies. *Biochemical Society Transactions*, *38*(4), 993–995. https://doi.org/10.1042/BST0380993

LaFerla, F. M., & Green, K. N. (2012). Animal models of Alzheimer disease. *Cold Spring Harbor Perspectives in Medicine*, *2*(11). https://doi.org/10.1101/cshperspect.a006320

LaFerla, F. M., Tinkle, B. T., Bieberich, C. J., Haudenschild, C. C., & Jay, G. (1995). The Alzheimer's A beta peptide induces neurodegeneration and

apoptotic cell death in transgenic mice. *Nature Genetics*, *9*(1), 21–30. https://doi.org/10.1038/ng0195-21

Lambert, J. C., Ibrahim-Verbaas, C. A., Harold, D., Naj, A. C., Sims, R., Bellenguez, C., Amouyel, P. (2013). Meta-analysis of 74,046 individuals identifies 11 new susceptibility loci for Alzheimer's disease. *Nature Genetics*, *45*(12), 1452–8. https://doi.org/10.1038/ng.2802

Lewis, P. a, Piper, S., Baker, M., Onstead, L., Murphy, M. P., Hardy, J., Golde, T. E. (2001). Expression of BRI-amyloid beta peptide fusion proteins: a novel method for specific high-level expression of amyloid beta peptides. *Biochimica et Biophysica Acta*, *1537*(1), 58–62. https://doi.org/S0925-4439(01)00054-0 [pii]

Lin, H. A. I., Bhatia, R., & Lal, R. (2001). Amyloid beta protein forms ion channels: implications for Alzheimer's disease pathophysiology. *Faseb J*, *15*(13), 2433–2444. https://doi.org/10.1096/fj.01-0377com

Ling, D., Magallanes, M., & Salvaterra, P. M. (2014). Accumulation of amyloid-like Aβ1-42 in autophagy-endosomal-lysosomal (AEL) vesicles: Potential implications for plaque biogenesis. *ASN Neuro*, *6*(2), 95–109. https://doi.org/10.1042/AN20130044

Liu, C.-C., Liu, C.-C., Kanekiyo, T., Xu, H., & Bu, G. (2013). Apolipoprotein E and Alzheimer disease: risk, mechanisms and therapy. *Nature Reviews. Neurology*, *9*(2), 106–18. https://doi.org/10.1038/nrneurol.2012.263

Liu, Z., Li, T., Li, P., Wei, N., Zhao, Z., Liang, H., Wei, J. (2015). The Ambiguous

Relationship of Oxidative Stress, Tau Hyperphosphorylation, and Autophagy Dysfunction in Alzheimer's Disease. *Oxidative Medicine and Cellular Longevity*, *2015*. https://doi.org/10.1155/2015/352723

Martinez-Vicente, M. (2015). Autophagy in neurodegenerative diseases: From pathogenic dysfunction to therapeutic modulation. *Seminars in Cell and Developmental Biology*, *40*, 115–126. https://doi.org/10.1016/j.semcdb.2015.03.005

McGowan, E., Eriksen, J., & Hutton, M. (2006). A decade of modeling Alzheimer's disease in transgenic mice. *Trends in Genetics*, *22*(5), 281–289. https://doi.org/10.1016/j.tig.2006.03.007

Meli, G., Lecci, A., Manca, A., Krako, N., Albertini, V., Benussi, L., Cattaneo, A. (2014). Conformational targeting of intracellular Aβ oligomers demonstrates their pathological oligomerization inside the endoplasmic reticulum. *Nature Communications*, *5* (May), 3867. https://doi.org/10.1038/ncomms4867

Nixon, R. A. (2006). Autophagy in neurodegenerative disease: friend, foe or turncoat? *Trends in Neurosciences*, *29*(9), 528–535. https://doi.org/10.1016/j.tins.2006.07.003

Oddo, S., Caccamo, A., Smith, I. F., Green, K. N., & LaFerla, F. M. (2006). A Dynamic Relationship between Intracellular and Extracellular Pools of Aβ. *The American Journal of Pathology*, *168*(1), 184–194. https://doi.org/10.2353/ajpath.2006.050593

Saito, T., Matsuba, Y., Mihira, N., Takano, J., Nilsson, P., Itohara, S., Saido, T.

C. (2014). Single App knock-in mouse models of Alzheimer's disease. *Nat Neurosci*, *17*(5), 661–663. https://doi.org/10.1038/nn.3697

Schindelin, J., Arganda-Carreras, I., Frise, E., Kaynig, V., Longair, M., Pietzsch, T., Cardona, A. (2012). Fiji: an open-source platform for biological-image analysis. *Nature Methods*, *9*(7), 676–682. https://doi.org/10.1038/NMETH.2019

Selkoe, D. J., & Hardy, J. (2016). The amyloid hypothesis of Alzheimer's disease at 25 years. *EMBO Molecular Medicine*, *8*(e201606210), 1–14. https://doi.org/10.15252/emmm.201606210

Serrano-Pozo, A., Frosch, M. P., Masliah, E., & Hyman, B. T. (2011). Neuropathological alterations in Alzheimer disease. *Cold Spring Harbor Perspectives in Medicine*, *1*(1). https://doi.org/10.1101/cshperspect.a006189

Sisodia, S. S. (1992). Beta-amyloid precursor protein cleavage by a membrane-bound protease. *Proceedings of the National Academy of Sciences of the United States of America*, *89*(13), 6075–9. https://doi.org/10.1073/pnas.89.13.6075

Soto, C., Brahes, M. C., Alvarez, J., & Inestrosa, N. C. (1994). Structural Determinants of the Alzheimer's. *J. Neurochem.*, *63*, 1191.

Studer, L., Vera, E., & Cornacchia, D. (2015). Programming and Reprogramming Cellular Age in the Era of Induced Pluripotency. *Cell Stem Cell*, *16*(6), 591–600. https://doi.org/10.1016/j.stem.2015.05.004

Vardy, E. R. L. C., Catto, A. J., & Hooper, N. M. (2005). Proteolytic mechanisms

in amyloid-β metabolism: Therapeutic implications for Alzheimer's disease. *Trends in Molecular Medicine*, *11*(10), 464–472. https://doi.org/10.1016/j.molmed.2005.08.004

Virginia M.-Y. Lee, Brian J. Balin, Laszlo Otvos, J. and J. Q. T. (1991). A68: A Major Subunit of Paired Helical Filaments and Derivatized Forms of Normal Tau. *Science*, *251*(4994), 675–678.

Weggen, S., & Beher, D. (2012). Molecular consequences of amyloid precursor protein and presenilin mutations causing autosomal-dominant Alzheimer's disease. *Alzheimer's Research & Therapy*, *4*(2), 9. https://doi.org/10.1186/alzrt107

Yagi, T., Ito, D., Okada, Y., Akamatsu, W., Nihei, Y., Yoshizaki, T., Suzuki, N. (2011). Modeling familial Alzheimer's disease with induced pluripotent stem cells. *Human Molecular Genetics*, *20*(23), 4530–4539. https://doi.org/10.1093/hmg/ddr394

Yang, J., Li, S., He, X.-B., Cheng, C., & Le, W. (2016). Induced pluripotent stem cells in Alzheimer's disease: applications for disease modeling and cell-replacement therapy. *Molecular Neurodegeneration*, *11*(1), 39. https://doi.org/10.1186/s13024-016-0106-3

Zheng, H., & Koo, E. (2011). Biology and pathophysiology of the amyloid precursor protein. *Molecular Neurodegeneration*, *6*(1), 27. https://doi.org/10.1186/1750-1326-6-27